HHS Public Access

Author manuscript

Cell Rep. Author manuscript; available in PMC 2021 February 04.

Published in final edited form as:

Cell Rep. 2020 August 18; 32(7): 108037. doi:10.1016/j.celrep.2020.108037.

Affinity for the Interface Underpins Potency of Antibodies Operating In Membrane Environments

Edurne Rujas[1,2,14], **Sara Insausti**[1,14], **Daniel P. Leaman**[3], **Pablo Carravilla**[1,4,5], **Saul González-Resines**[6], **Valérie Monceaux**[7], **Rubén Sánchez-Eugenia**[1], **Miguel García-Porras**[1], **Ibon Iloro**[8], **Lei Zhang**[3], **Félix Elortza**[8], **Jean-Philippe Julien**[2,9,10], **Asier Saéz-Cirión**[7], **Michael B. Zwick**[3], **Christian Eggeling**[4,5], **Akio Ojida**[11], **Carmen Domene**[6,12], **Jose M.M. Caaveiro**[13,*], **José L. Nieva**[1,15,*]

[1]Instituto Biofisika (CSIC, UPV/EHU) and Department of Biochemistry and Molecular Biology, University of the Basque Country (UPV/EHU), PO Box 644, 48080 Bilbao, Spain

[2]Program in Molecular Medicine, The Hospital for Sick Children Research Institute, Toronto, ON M5G 0A4, Canada

[3]Department of Immunology and Microbiology, The Scripps Research Institute, La Jolla, CA 92037, USA

[4]Institute of Applied Optics and Biophysics Friedrich-Schiller-University Jena, Max-Wien Platz 4, 07743 Jena, Germany

[5]Leibniz Institute of Photonic Technology e.V., Albert-Einstein-Straße 9, 07745 Jena, Germany

[6]Department of Chemistry, University of Bath, Claverton Down, Bath BA2 7AX, UK

[7]Institut Pasteur, Unité HIV Inflammation et Persistance, 28 rue du Docteur Roux, 75724 Paris Cedex 15, France

[8]Proteomics Platform, CIC bioGUNE, Parque Tecnológico de Vizcaya, 48160 Derio, Spain

[9]Department of Biochemistry, University of Toronto, Toronto, ON M5S 1A8, Canada

[10]Department of Immunology, University of Toronto, Toronto, ON M5S 1A8, Canada

[11]Department of Chemical Biology, School of Pharmaceutical Sciences, Kyushu University, Fukuoka 819-0395, Japan

[12]Department of Chemistry, University of Oxford, Oxford OX1 3TF, UK

*Correspondence: jose@phar.kyushu-u.ac.jp (J.M.M.C.), joseluis.nieva@ehu.es (J.L.N.).

AUTHOR CONTRIBUTIONS

E.R., S.I., J.M.M.C., and J.L.N. designed research. E.R., S.I., D.P.L., C.D., S.G.-R., V.M., P.C., I.I., M.G.-P., L.Z., and A.O. performed research. E.R., S.I., D.P.L., V.M., P.C., I.I., R.S.-E., C.E., F.E., J.-P.J., A.S.-C., M.B.Z., A.O., C.D., J.M.M.C., and J.L.N. analyzed data. E.R., S.I., J.M.M.C., and J.L.N. wrote the paper with input from all authors.

SUPPLEMENTAL INFORMATION

Supplemental Information can be found online at https://doi.org/10.1016/j.celrep.2020.108037.

DECLARATION OF INTERESTS

A patent application covering several aspects of this work has been filled by Kyushu University/UPV-EHU/CSIC/FBB, listing E.R., R.S.-E., A.O., J.L.N., and J.M.M.C. as inventors.

[13]Laboratory of Global Health Care, School of Pharmaceutical Sciences, Kyushu University, Fukuoka 819-0395, Japan

[14]These authors contributed equally

[15]Lead Contact

SUMMARY

The contribution of membrane interfacial interactions to recognition of membrane-embedded antigens by antibodies is currently unclear. This report demonstrates the optimization of this type of antibodies via chemical modification of regions near the membrane but not directly involved in the recognition of the epitope. Using the HIV-1 antibody 10E8 as a model, linear and polycyclic synthetic aromatic compounds are introduced at selected sites. Molecular dynamics simulations predict the favorable interactions of these synthetic compounds with the viral lipid membrane, where the epitope of the HIV-1 glycoprotein Env is located. Chemical modification of 10E8 with aromatic acetamides facilitates the productive and specific recognition of the native antigen, partially buried in the crowded environment of the viral membrane, resulting in a dramatic increase of its capacity to block viral infection. These observations support the harnessing of interfacial affinity through site-selective chemical modification to optimize the function of antibodies that target membrane-proximal epitopes.

Graphical Abstract

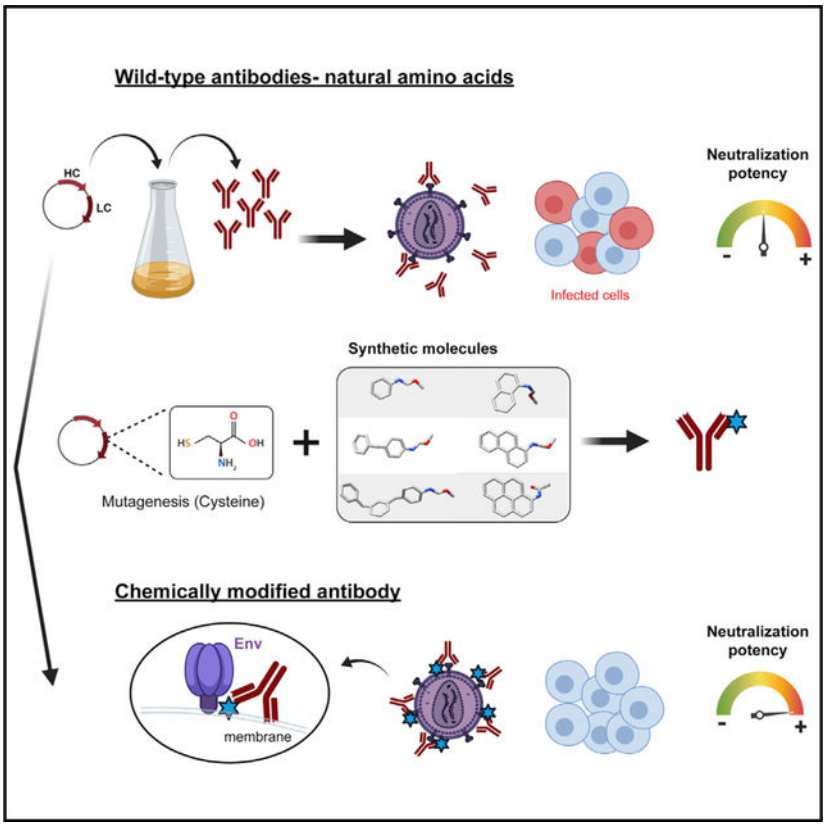

In Brief

Rujas et al. describe the site-selective chemical modification of antibodies to improve the molecular recognition of epitopes at membrane surfaces. The modification using aromatic compounds dramatically enhanced the virus neutralization potency and native antigen binding efficiency of HIV-1 antibodies directed against the membrane-embedded MPER epitope.

INTRODUCTION

Chemical modification of proteins is a method widely used to engineer proteins and to elucidate their function in the cell (Isenegger and Davis, 2019; Krall et al., 2016; Sakamoto and Hamachi, 2019). In antibodies (Abs), chemical modifications are generally introduced to link the protein to a second molecule to generate functionality, such as in Ab-drug conjugates, or to label the protein for analytical purposes. In addition, site-selective chemical modification provides a potential route to optimize Ab function beyond the limits imposed by the collection of natural amino acids (Isenegger and Davis, 2019; Krall et al., 2016; Sakamoto and Hamachi, 2019). Here, we sought to improve Ab recognition of integral membrane antigens by site-specific chemical conjugation of synthetic aromatic compounds.

Integral membrane proteins represent one of the largest fraction of antibody-based therapeutic targets under clinical evaluation, including tumor-associated antigens such as the tetraspanin CD20, or members of several receptor families such as the human epidermal growth factor receptor tyrosine kinase and the tumor necrosis factor-related apoptosis-inducing ligand receptors (Hendriks et al., 2017), diverse families of ion-channels (Hutchings et al., 2019), G-protein-coupled receptors (Hutchings et al., 2017), and viral glycoproteins from relevant human pathogens, such as the Ebola virus or the human immunodeficiency virus type-1 (HIV-1) (Walker and Burton, 2018). Many Abs targeting these integral membrane-antigens reportedly bind to membrane-proximal regions, i.e., epitopes that are exposed close to, or lying on the membrane surface (Flyak et al., 2018; Hutchings et al., 2017; Klein et al., 2013; Lee et al., 2020; Pahuja et al., 2018; Xu et al., 2005).

The membrane-proximal epitope MPER, existing in the HIV-1 envelope glycoprotein Env, epitomizes this class of antigen determinant (Huang et al., 2012; Krebs et al., 2019; Pinto et al., 2019; Rantalainen et al., 2020; Stiegler et al., 2001; Williams et al., 2017; Zhang et al., 2019). One Ab that binds to this region, 10E8, has been extensively studied both structurally and functionally (Huang et al., 2012; Irimia et al., 2017; Lee et al., 2016; Rantalainen et al., 2020; Rujas et al., 2016) and thus is a relevant candidate for rational optimization by protein engineering. Effective binding of 10E8 to Env translates into viral neutralization, hence, higher affinity of this Ab for the antigen would result in greater capacity to block cell infection (Carravilla et al., 2019). The evidence accumulated so far suggests that engagement of Env by 10E8 requires not only the recognition of the proper protein epitope, but also additional contacts to adjust the Ab surface to the viral membrane interface (Irimia et al., 2016, 2017; Lee et al., 2016; Rantalainen et al., 2020; Rujas et al., 2016). Recent studies reported by us and others have demonstrated that the neutralization potency of this Ab can be improved ~10-fold by mutating residues located at the contact interface with the

viral membrane (Kwon et al., 2018; Rujas et al., 2018). Furthermore, super-resolution microscopy studies of intact virions have revealed that the affinity of these mutated antibodies for native Env increased (Carravilla et al., 2019). In other words, optimal accommodation of the viral membrane onto the Ab surface is a critical aspect for efficient viral neutralization.

Here, we have examined the hypothesis that 10E8-like Abs can be rationally optimized by grafting synthetic aromatic compounds at sites that, while remote from the epitope-binding site, may facilitate its interaction with the viral membrane. The antibody was specifically modified with iodoacetamide derivatives at specific places predicted to improve the interaction of 10E8 with the viral membrane. As a result, the biological function of the modified antibody increased dramatically using various benchmark methodologies and biological assays. Following the same strategy, mutants of 10E8 of reduced efficacy and a less potent Ab arising from a different lineage were also modified achieving much greater potency. Collectively, our data provide a proof-of-principle to support site-selective conjugation with aromatic compounds as a rational approach to improve Ab recognition of epitopes that are located at membrane interfaces.

RESULTS

Strategy to Optimize Antibody 10E8 by Chemical Modification with Aromatic Compounds

Our rational approach seeks the promotion of interfacial affinity of the surface of the anti-HIV Ab 10E8 that comes into contact with the viral membrane during epitope recognition (Figures 1A and S1A). The specific positions selected for modification were the surface-exposed residue H.W100b at HCDR3, and a residue distant from the epitope binding pocket, L.S65, as structure-based analyses suggested that these residues insert to some degree into the membrane interface upon binding to the epitope (Figure 1A). To carry out the chemical modification, 10E8 Fab was first engineered to contain a single Cys residue at each position (L.S65C and H.W100bC mutants). Interaction of the selected residues with the membrane upon binding to the epitope was probed by conjugation of the introduced Cys residues with the fluorescent polarity-sensitive probe 7-nitrobenz-2-oxa-1,3-diazol-4-yl (NBD) (Figure S1B). The NBD fluorescence emission of these two labeled mutants increased significantly in the presence of proteoliposomes, in contrast to the absence of change of signal when the Fab was modified at a site distant from the membrane.

We next sought to optimize 10E8 interactions with the viral membrane through chemical modification with aromatic compounds, because this class of chemical groups has a tendency to engage the interfacial region of the lipid bilayer (McDonald and Fleming, 2016; White et al., 2001; White and Wimley, 1999; Wimley and White, 1996; Yau et al., 1998). We selected two different classes of synthetic aromatic compounds for antibody modification (Figure 1B). First, a series of molecules containing phenyl moieties linked via flexible spacers of increasing length were obtained. These linear-flexible compounds, designated as Lin1, Lin2, and Lin3, were expected to differentially contribute to the peripheral membrane interaction depending on their length. Second, polycyclic aromatic compounds, similar in size (naphthyl group, Fus2) or bulkier (pyrenyl group, Fus4) than that of the indole group of Trp, were also obtained. These bulk-rigid molecules were predicted to accommodate at the

water-membrane interface and not within the disordered acyl regions (Hoff et al., 2005; Loura et al., 2013). Furthermore, their quadrupole moments augment with the number of fused rings, presumably benefiting their interaction with the complex environment of the membrane interface (McDonald and Fleming, 2016; Yau et al., 1998). All these compounds were obtained as the iodoacetamide derivative for readily modification of a Cys introduced by site-directed mutagenesis.

The Ab subject to chemical modification, 10E8, binds to its epitope embedded in the HIV membrane. Thus, MD simulations in bilayers made of a virus-like (VL) lipid mixture (Huarte et al., 2016) (see STAR Methods) were carried out to confirm that the synthetic aromatic moieties interact with the highly packed viral membrane (Figures 1C, S2, and S3; Table S1). MD simulations in bilayers made of the lipid POPC were employed as reference (Figure S3; Table S1). The MD simulations showed a tendency of the selected compounds for partitioning from an aqueous environment into the viral membrane interface and revealed a distinctive distribution according to their molecular shape and rigidity.

Chemical modification of the Fab with these compounds at the selected positions was obtained by treating the Fab portion of the antibody with iodoacetamide synthetic derivatives. Conjugation was verified for the most hydrophobic and bulkier compounds of each series (i.e., Lin3 and Fus4) by mass spectrometry (Figure S4A). These modifications did not appreciably diminish the thermostability, the secondary structure composition of the antibody, or their ability to recognize the epitope peptide in ELISA (Figures S4B and S4C; Table S2).

Aromatic Grafting Enhances 10E8 Anti-Viral Potency

We next performed a functional screening using Fabs chemically modified with the aromatic compounds against two HIV-1 pseudoviruses (PsVs) bearing Env JRCSF (Tier-2) or PVO.4 (Tier-3), which display different degrees of sensitivity to the Ab 10E8 (Figure 2). Some of the compounds induced a dramatic increase in potency, as determined by the abrupt reduction of doses required to block virus entry into cells (IC_{50} values) with respect to the wild-type (WT) Fab.

The modification with the linear compounds Lin1, Lin2, and Lin3 at position L.S65C significantly increased the potency of 10E8 (Figure 2A, left, black traces in dose-response curves). The modifications with the longest compounds Lin2 or Lin3 were more effective (ca. 20- to 30-fold more potent than WT antibody) whereas Lin1 did not induce significantly greater inhibition than the unmodified antibody. When the antibody was modified with the polycyclic compounds Fus2 and Fus4, widely different observations were made (Figure 2A, left, red traces in dose-response curves). Whereas modification with Fus2 led to small improvements with respect to WT antibody and comparable to introducing a Trp at that position, the inhibitory potency of 10E8 modified with Fus4 resulted in a dramatic potentiation (>80- to 100-fold), far beyond our initial expectations. These results indicate that synthetic compounds linked to the Fab surface that accommodates the membrane enhance the functional performance of 10E8, beyond the level attainable by mutation with the natural amino acid Trp.

Chemical modifications at H.W100bC of the HCDR3 had a lower effect more complex to analyze (Figure 2A, right). The modification with the shortest and longest linear compounds, Lin1 and Lin3, decreased the potency of the antibody, whereas the modification with Lin2, of intermediate length, enhanced the potency of the Fab, but only to a small degree. The increase in potency achieved by modification with Fus4 of residue H.W100b is much less marked than that observed at the L.S65 position, although still significant (ca. 5-fold), specially taking into account the proximity of this residue to the key region recognizing the epitope peptide and its environment, and the fact that the substituted Trp residue is itself a large aromatic residue. The modification of the same position with Fus2 mostly recapitulated the activity of the WT Fab, underscoring the idea that the nature of the compound is relevant for the level of Ab optimization.

These results are summarized in Figure 2B. Our approach identified aromatic compounds Lin2, Lin3, and Fus4 as robust enhancers of 10E8 anti-viral activity, when placed at a region that remains proximal to the viral membrane in the Fab-epitope complex. Moreover, we found that the chemical modification of this area with Fus4 led to an extremely potent Ab 10E8. The smaller and heterogeneous effect of the modification at the tip of HCDR3 compared to that at the membrane-proximal area is consistent with a greater sensitivity of the Ab when being modified in the epitope recognition loop (Rujas et al., 2016).

Chemical Modification with Aromatic Compounds Enhances Suppression of Primary Virus Infection

We next corroborated the functional improvement generated by the chemical modification with aromatic compounds in an experimental setting relevant for the natural infection process (Figure 3). To that end, we measured the antiviral effect of WT and chemically modified Fabs in viral infection assays by using primary host cells and the infectious CCR5-tropic HIV-1 BaL strain. Primary $CD4^+$ T cells isolated from donors have heterogeneous susceptibility to HIV-1 infection and are less permissive to Env-mediated cell entry than TZM-bl cells overexpressing viral receptor CD4 and co-receptor CCR5 (Wei et al., 2002), thus providing a culture system more relevant for the natural process of HIV-induced cell infection.

$CD4^+$ T cells were isolated from fresh peripheral blood mononuclear cells (PBMCs) from different donors, activated during 3 days with phytohemagglutinin-L and IL2, and challenged with a fixed infectious dose of R5 HIV-1 (BaL) (Sáez-Cirión et al., 2010; Valle-Casuso et al., 2019) in the presence or absence of the Fabs. As expected, $CD4^+$ T cells from different donors displayed different levels of susceptibility to HIV infection, as inferred from intracellular HIV-1 Gag levels at day 3 after infection (Figure 3A). 10E8 Fabs conjugated with the compounds Lin3 and Fus4 exhibited more potent antiviral activity than the WT Fab, independently of the level of infection achieved on the $CD4^+$ T cells in the absence of Fabs (Figure 3B). As in the cell-entry inhibition assays, modification with compound Fus4 appeared to have a more marked effect than Lin3.

Mechanistic Insights and Specificity of the Potentiation Effect

To gain insights into the specificity and mechanism underlying the increase in Ab potency after site-selective chemical modification, we next explored the effects of the most potent compound Fus4 in a variety of experimental conditions (Figures 4 and S5). First, to rule out potential site-dependent interactions not mediated by membrane, we determined the effects of Fus4 placed at different positions on the 10E8 surface that accommodates the viral membrane. The selected positions L.S30, L.N52, and L.S65 were all distant from the MPER epitope (alpha-carbons at 14, 18, and 22Å from the epitope, respectively) (Figures 4A and S5A). As a control for no-interaction with the membrane, we also tested the effect of Fus4 linked to the C-terminal residue H.C216, which is predicted to remain exposed to the aqueous solution upon engagement with the MPER epitope. These positions were modified with the Fus4 one by one and the activities of the resulting chemically modified variants compared in cell-entry inhibition assays (Figure 4B). As expected from the absence of membrane insertion, modification with Fus4 at residue H.C216 had no effect on the activity of the Ab. For the rest of the positions, L.S30, L.N52, and L.S65, the observed functional improvements were comparable to each other, suggesting that a particular location of the chemical modification at the membrane-accommodating area is not important to improve the anti-viral function of 10E8.

Chemical conjugation with Fus4 was also efficient in the context of a paratope that has been altered by classical site-directed mutagenesis to reduce the activity of 10E8 (Figure 4C). The mutation H.W100bG removes the side chain of the Trp residue at the tip of the HCDR3, producing a substantial reduction of the antiviral activity of 10E8 (Carravilla et al., 2019; Rujas et al., 2016). Thus, we performed cell-entry assays to establish whether adding Fus4 at a distant site through chemical conjugation could rescue functionally the mutation at the tip of the HCDR3 loop. As shown in Figure 4C, Fus4 linked at L.S65C position also increased the activity of the deficient H.W100bG mutant.

We also investigated the effect of attaching Fus4 to Abs already engineered to increase their potency (Figure S5). The effect of the chemical modification is not additive, because the incorporation of a second molecule of Fus4 within the membrane-proximal Ab region did not result in greater neutralization potency (Figures S5A and S5B). However, the attachment of Fus4 to an electrostatically optimized 10E8 Fab resulted in a certain degree of potentiation of the antiviral activity (Figures S5C–S5E). The 3R 10E8 mutant combines substitutions S30R, N52R, and S67R at the surface where the antibody accommodates the viral membrane. These mutations were rationally designed to enhance the electrostatic interactions between the Fab and the membrane (Carravilla et al., 2019; Rujas et al., 2018). Notably, the combination of this triple mutation with the Fus4-based chemical modification, rescued completely the loss of activity of the poorly active variant bearing the H.W100bG mutation at the epitope-binding site.

Together, these observations highlight a significant flexibility to introduce chemical modifications at various positions of the membrane-proximal region of 10E8, but they also highlight the difficulty to attain additive effects by combining modifications at multiple sites. Notably, they also suggest that chemical modification can functionally complement a deleterious mutation introduced at the distant epitope-binding site.

Assuming that membrane compositions of different HIV-1 isolates are comparable, we next tested whether the potentiation effect observed for L.S65C-Fus4 10E8 could be extended to a wide range of Env antigens (Table 1; Figure S6). To that end, antiviral activity of 10E8 L.S65C-Fus4 was evaluated against a PsV panel of eight HIV-1 isolates used previously as an indicator of cross-clade neutralization breadth (Simek et al., 2009). A decrease in IC_{50} was observed with all tested isolates when comparing the chemically modified 10E8 variant L.S65C-Fus4 to 10E8-WT, ranging between 10- and 700-fold with a mean value of >200-fold (Table 1). In addition, to make sure that this remarkable potency enhancement was due to improved recognition of the specific target HIV-1 Env, and not to some off-target, unspecific effects, we also tested the antiviral activities of the Fabs 10E8 WT and S65C-Fus4 against HIV-2 and SIV used as negative controls (Table 1; Figure S6). We did not detect any neutralization against the negative controls in these assays, thereby confirming the specific activity of the chemically modified Fab. In conjunction, these results provide support that chemical modification with compound Fus4 confers Ab 10E8 higher, but specific, antiviral efficacy against a broad collection of HIV-1 Env isolates.

Aromatic Grafting Stimulates Binding to the Integral Membrane Antigen

To gain further insights into the molecular basis explaining the antiviral potentiation of 10E8, we next determined the effects of chemical modification with Fus4 on the antigen-binding function of the Ab (Figure 5). We employed quantitative super-resolution fluorescence stimulated emission depletion (STED) microscopy as previously reported (Carravilla et al., 2019), to establish whether grafting Fus4 affects the binding of the antibody to native Env in intact virions (Figures 5A and 5B). STED microscopy provides mechanistic information at two levels (Carravilla et al., 2019). First, by detecting the fluorescent foci over the virion surface, one can determine the number of Env clusters recognized by the Abs. Thus, this technique has the potential to monitor off-target Ab interactions that might occur with membrane areas devoid of antigen. And second, emission intensity analyses on the virion images allow the quantitative comparison of affinities toward the integral membrane-antigen of modified versus unmodified Abs. Due to the linear nature of STED, the number of photons emitted is proportional to the number of fluorescent molecules.

Figure 5A displays micrographs of individual eGFP-labeled viral particles incubated with Fab 10E8 WT or chemically modified Fab 10E8 L.S65C-Fus4 (top panels). Binding to Env on the viral particles was visualized using a secondary dye-labeled Ab. In this setting, the Ab/Env complexes were visualized in the super-resolved STED microscopy mode (magenta), whereas the eGFP signal was recorded in conventional confocal mode to identify the individual viral particles (green). Analysis of the punctate pattern revealed the number of antibodies/Env foci per virus, whose distribution was similar for Abs WT and L.S65C-Fus4, demonstrating similar engagement with clustered Env (Figure 5A, lower panels). In the absence of Env (Env(–) particles), the modified antibody did not engage with the viral membrane as evidenced by the lack of antibody signal (Figure 5A, middle panels). Analysis of the signal intensity in every individual virion revealed an increased binding to Env for L.S65C-Fus4 compared to the WT Ab. In contrast, the signal on the Env(–) particles was undistinguishable from the background signal (Figure 5B).

The absence of Ab signal in particles devoid of Env reveals an important mechanistic aspect (i.e., that the chemical modification does not promote spontaneous partitioning of the Ab into the bare viral membrane). This conclusion was further supported by experiments employing VL model vesicles, which confirmed that Fus4 can spontaneously insert into membranes in the free form, but not appreciably as part of the Fab-Fus4 conjugate (Figure S7). Thus, even if Fus4 was by itself capable to partition into VL membranes, both in simulations and in an experimental set-up, the small modification of the Fab (<1% of its total mass) does not confer the capacity for spontaneous insertion into the viral membrane to the Ab-Fus4 conjugate.

Even though 10E8 is generally assumed not to be polyreactive in comparison with other MPER-targeting Abs (Huang et al., 2012), and despite the subtle effect exerted by the modification on membrane partitioning *in vitro*, the possibility of Fab 10E8 L.S65C-Fus4 interacting nonspecifically with more complex cell structures could not be excluded. Thus, we also tested the polyreactivity and cytotoxicity upon incubation of the chemically modified Fab with cells (Figures 5C and 5D). In the polyreactivity assay, a dim fluorescence signal above background was observed in the HEp-2 cells incubated with the Fab 10E8 L.S65C-Fus4, suggesting that the chemical modification results in low-level, non-specific Ab binding (Figure 5C). In contrast, the incubation with the chemically modified Fab appeared not to exert toxic effects on the TZM-bl host cells (Figure 5D).

Collectively, the results displayed in Figure 5 suggest that Fus4 effects on 10E8 function mostly operate during or after the specific recognition of the Env epitope by the paratope. These data also caution on the possible off-target effects when dealing with complex biological matrices (see Discussion below).

Successful Modification of a Second Antibody

To prove the effectiveness of functional optimization with Fus4 in the context of a paratope arranged differently, we next examined the effects induced by grafting this compound in an Ab arising from a different lineage. Although less potent, the HIV antibody 4E10 also embodies a surface that accommodates the viral membrane in Fab-epitope complexes, which in this case is composed by heavy-chain residues (Irimia et al., 2016; Rujas et al., 2017). A chemically modified version of 4E10 was prepared following an analogous approach to that of antibody 10E8 (Figure 6A; Table S2). In parallel, we studied the effect of chemical modification with Fus4 on a deletion mutant in which the HCDR3 apex was ablated (termed ΔLoop, Figure 6B) (Rujas et al., 2015). This mutant is characterized by the complete absence of neutralizing activity and lack of binding ability to the native, integral membrane antigen Env (Carravilla et al., 2019).

Despite the different docking angle of 4E10 to the helical epitope-peptide, and the different Fab chain that composes the membrane-proximal area with respect to 10E8, modification with Fus4 also enhanced the antiviral potency of 4E10 to a great extent (Figure 6C). Remarkably, introducing a single chemical modification with Fus4 (also at H.S28) was sufficient to fully rescue the inhibitory potency of the inactive ΔLoop mutant to levels comparable to those of WT (Figure 6C).

We investigated if antibody optimization with Fus4 was also correlated with an increased binding of 4E10 to native Env by using STED microscopy (Figures 6D and 6E). Similarly to the results presented in Figure 5A for the modification of 10E8, STED microscopy data for 4E10 displayed individual puncta of antibody-Env complexes (Figure 6D), whose intensity analysis confirmed that the functional improvement induced by site-specific modification with Fus4 correlated with an increase in binding to native Env on virions (Figure 6E). Furthermore, the functionally restored, chemically modified ΔLoop variant, showed levels of Env binding comparable to those measured for the WT 4E10 (Figures 6D and 6E). Here again, signal on the Env(–) particles was only background-like.

DISCUSSION

Approaches to Ab optimization are generally based on (and limited by) modifications with function-enhancing natural amino acid residues. In this work, we sought to optimize the function of Abs that target integral membrane antigens with site-selective chemical modification, using rationally designed synthetic molecules (Krall et al., 2016), thus unconstrained by the restrictions when only using natural amino acid residues. The Ab subject for modification, 10E8, contains a surface to accommodate the viral membrane in the formation of the Ab-antigen complex (Irimia et al., 2017; Kwon et al., 2018; Lee et al., 2016; Rantalainen et al., 2020; Rujas et al., 2016, 2018). To improve affinity and antiviral function of the Ab, we attached at selected sites of this surface aromatic compounds, which were selected and designed on the basis of their capacity for partitioning from water into membranes and the preferential interactions that they stablish with the different regions of the lipid bilayer (White et al., 2001; White and Wimley, 1999; Wimley and White, 1996).

MD simulations demonstrated that the selected compounds partition from the aqueous solution into lipid bilayers that emulate the rigid viral membrane, where they distribute according to their properties. Rigid polycyclic aromatic compounds Fus2 and Fus4 adopted a shallow location oriented parallel to the bilayer normal, whereas linear compounds Lin1, Lin2, and Lin3 distributed homogeneously across the bilayer with no-preferential orientation. We successfully showed that chemical modification with the two different classes of synthetic compounds, at rationally designated sites, increased significantly the potency of the Ab 10E8.

Functional screenings and evaluation of the effects on the biological activity of the Ab provided information relevant for understanding the possible mechanisms underlying the effectiveness of the procedure. Chemical modification with the bulkiest and rigid molecule Fus4 generated an extremely potent 10E8 Ab. The modification involves the addition, at a single position, of a synthetic molecule ≤300 Da. The extent of the resulting modification is very small in comparison to the size of the antibody, and yet the effect on Ab function was remarkable (more than two orders of magnitude in standard neutralization assays). We hypothesize that the comparatively higher efficacy of this compound might be originated from the combination of its hydrophobicity and orientation at the water-membrane interface, which could contribute to stabilize the docking of the Ab to the helical epitope with a favorable geometry. This favorable arrangement might correspond to one of the conformational states visited by the pre-fusion Env glycoprotein (Carravilla et al., 2019;

Munro et al., 2014). In this regard, it is tempting to speculate that binding of the chemically optimized Fab would induce more favorably an initial tilting of Env relative to the membrane surface, and/or subsequently stabilize the trimer in a position lifted off the membrane (Rantalainen et al., 2020). Alternatively and/or complementary, the favorable membrane partition characteristics could facilitate the transient residence of the Ab at the membrane interface promoting the recognition of the epitope.

The applicability of this procedure was further demonstrated with a second Ab, 4E10, which was modified by analogous strategy and principles. Notably, the efficacy of this approach is such that it did not only improve the potency of the WT antibody by chemical modification with Fus4, but also rescued a completely inactive variant (termed ΔLoop) to WT-like neutralization levels. In view of these evidences, we conclude that promoting favorable interactions with the membrane interface through chemical modification with synthetic aromatic compounds could be a more general procedure for potentiating the molecular recognition of membrane-proximal epitopes.

This class of epitopes has been found in relevant therapeutic targets, including other viral glycoproteins, tumor-associated antigens, ion-channels, and G protein-coupled receptors. The optimization strategy described herein could be employed to analyze the structure-function relationships of integral membrane antigens and the Ab adaptations conducive to their molecular recognition at membrane surfaces. A potential drawback of this methodology employing compounds with a greater tendency to partition in membranes is the increase of unspecific binding of the antibody to membranes, which could possibly compromise binding specificity in living tissues, and, therefore, its straightforward clinical use. We surmise that in those cases, additional protein and/or chemical engineering cycles seeking to promote functional efficacy, while driving down putative off-target effects, may be necessary.

In summary, chemical modification dramatically improves the performance of anti-HIV-1 antibodies potentially providing a tool to inform vaccine and immunotherapeutic Ab design. Moreover, we believe site-selective chemical modification using aromatic compounds may be employed to optimize not only Abs acting at or near biological membranes but other types of Abs and even other classes of proteins and peptides of various functions and therapeutic profiles.

STAR★METHODS

RESOURCE AVAILABILITY

Lead Contact—Further information and requests for resources and reagents should be directed to and will be fulfilled by the Lead Contact, Jose Nieva (joseluis.nieva@ehu.es)

Materials Availability—All unique/stable reagents generated in this study are available from the Lead Contact with a completed Materials Transfer Agreement

Data and Code Availability—This study did not generate any unique datasets or code.

EXPERIMENTAL MODEL AND SUBJECT DETAILS

T cell donors: Blood samples from were obtained from the French blood bank (Etablissement Français du Sang) as part of a collaboration agreement with the Institut Pasteur (C CPSL UNT, number 18/EFS/041). Anonymous, non-HIV-infected donors showed standard values of susceptibility to infection.

Escherichia coli T7-shuffle strain was grown in Luria Broth medium following the specifications of the supplier.

HEK293T and TZM-bl cells were cultured in DMEM (Dulbecco's Modified Eagle Medium), supplemented with 1 mM sodium pyruvate, 1 mM MEM Non-Essential Amino Acids Solution and 10% FBS, in a humidified incubator at +37°C, supplied with 5% CO_2.

METHOD DETAILS

Chemical compound synthesis—Compounds Lin1 and Fus4 were commercially available, whereas Compounds Lin2, Lin3, and Fus2 were produced by synthesis (reaction schemes and individual details of the synthetic procedure are indicated in Methods S1). Reagents and solvents were obtained from commercial suppliers and used without further purification, unless otherwise stated. Reactions were carried out under a positive atmosphere of nitrogen, unless otherwise stated. Reactions were monitored by thin layer chromatography (TLC) carried out on Merck TLC Silica gel 60 F_{254}, using shortwave UV light as the visualizing agent and phosphomolybdic acid in EtOH and heat as developing agent. Flash column chromatography was performed using Kanto Chemical Silica gel 60 N (spherical, 40–50 μm). ^{1}H NMR spectra were recorded on Varian Unity Plus 400 MHz spectrometer or Bruker Avance III HD 500 MHz spectrometer and were calibrated using residual undeuterated solvent as the internal references ($CDCl_3$: 7.26 ppm; MeOH-d_4: 3.31 ppm, acetone-d_6: 2.05 ppm; DMSO-d_6: 2.50 ppm). The following abbreviations were used to explain NMR peak multiplicities: s = singlet, d = doublet, t = triplet, q = quartet, p = pentet, m = multiplet, br = broad. Low-resolution and high-resolution mass spectra were recorded on Bruker micrOTOF focus II mass spectrometer using electrospray ionization time-of-flight (ESI-TOF) reflectron experiments.

Molecular Dynamics simulations in lipid bilayers—The preferred interactions and distributions of a series of the phenyl-based linear compounds (Lin1, Lin2, Lin3) and polycyclic aromatic compounds (Fus2 and Fus4) were studied in two model membranes: 1) a virus-like (VL) membrane made of 14% 1-palmitoyl-2-oleoylphosphatidylcholine (POPC), 16% 1-palmitoyl-2-oleoylphosphatidylethanolamine (POPE), 7% 1-palmitoyl-2-oleoyl phosphatidylserine (POPS), 17% N-palmitoyl sphingomyelin (PSM) and 46% cholesterol (Chol) (VL-3 surrogate of the viral membrane described in Huarte et al. [2016]); and 2) a neutral POPC bilayer that was used as standard reference (Wimley and White, 1996). Bilayers were built using CHARMM-GUI web with a surface area of 100 3 100Å2 (Jo et al., 2008). The lipid bilayers were solvated to produce a simulations box of 100 3 100 3 100Å3 composed of ~54,300 atoms for the POPC system and ~94,000 for the VL bilayer. 25 compound were introduced randomly in the water layers of the two systems. The system was neutralized with Sodium Chloride and a concentration of the 0.15 mM was set up. The

systems were run at a temperature of 298 K. A summary of the simulations with the produce time is shown in Table S1.

The software NAMD2.12 was employed to perform the molecular dynamics simulations (Phillips et al., 2005). The CHARMM36 force field was used to model the lipids and compound molecules (Klauda et al., 2010). Standard CHARMM parameters were used for ions (MacKerell et al., 1998), and the TIP3P model for water (Jorgensen et al., 1983). Pressure was maintained at 1 atm by a Langevin piston (Feller et al., 1995), with a damping time constant of 50 ps and a period of 100 ps. A semi-isotropic pressure coupling method was used in all the simulations. For the NAMD calculations, the pressure of the piston acted independently in each dimension, but maintained a constant ratio in the x,y axis, corresponding to the plane of the membrane. The temperature was maintained constant by coupling the system to a Langevin thermostat, with a damping coefficient of 5 ps^{-1}. The particle mesh Ewald (PME) algorithm was used for the evaluation of electrostatic interactions beyond 12Å, with a PME grid spacing of 1Å, and NAMD defaults for spline and k values (Darden et al., 1993).

Both electrostatics and van der Waals forces were smoothly switched off between the switching distance of 10Å and the cut-off distance of 12Å, using the default switching function in NAMD. A Verlet neighbor list with pair-list distance of 16Å was used to evaluate non-bonded neighboring forces within the pair-list distance (Verlet, 1967). The multi-time step algorithm Verlet-I/r-RESPA (Tuckerman et al., 1992; Verlet, 1967) was used to integrate the equations of motion. The timestep was set to 2 fs. The systems were subject to 10,000 steps of energy minimization.

Production and site-selective chemical modification of Fabs—Antibody Fab sequences were cloned in the plasmid pColaDuet and expressed in *Escherichia coli* T7-shuffle strain. Recombinant expression was induced at 18°C overnight with 0.4 mM isopropyl-D-thiogalactopyranoside when the culture reached an optical density of 0.8. Cells were harvested and centrifuged at 8,000 3 g, after which they were resuspended in a buffer containing 50 mM HEPES (pH 7.5), 500 mM NaCl, 35 mM imidazole, DNase (Sigma-Aldrich, St. Louis, MO) and an EDTA-free protease inhibitor mixture (Roche, Madrid, Spain). Cell lysis was performed using an Avestin Emulsiflex C5 homogenizer. Cell debris was removed by centrifugation, and the supernatant loaded onto a nickel-nitrilotriacetic acid (Ni-NTA) affinity column (GE Healthcare). Elution was performed with 500 mM imidazole, and the fractions containing the His-tagged proteins were pooled, concentrated, and dialyzed against 50 mM sodium phosphate (pH 8.0), 300 mM NaCl, 1 mM DTT, and 0.3 mM EDTA in the presence of purified protease Tobacco etch virus (Kawai et al., 2011). Fabs were separated from the cleaved peptides containing the His_6 tag by an additional step in a Ninitrilotriacetic column. The flow-through fraction containing the antibody was dialyzed overnight at 4°C against sodium acetate (pH 5.6) supplemented with 10% glycerol and subsequently loaded onto a MonoS ion exchange chromatography (IEC) column (GE Healthcare). Elution was carried out with a gradient of potassium chloride and the fractions containing the purified Fab concentrated and dialyzed against a buffer containing 10 mM sodium phosphate (pH 7.5), 150 mM NaCl, and 10% glycerol.

Site-selective fluorescence labeling and chemical conjugation was carried out as previously described (Carravilla et al., 2019; Heuck et al., 2000; Shepard et al., 1998). In brief, a cysteine-substituted Fab derivative was first generated by site-directed mutagenesis using the KOD-Plus mutagenesis kit (Toyobo, Osaka, Japan). Mutant Fabs bearing Cys residues at defined positions were subsequently modified with sulfhydryl-specific iodoacetamide derivatives of the polarity-sensitive probe NBD (Figure 1A) or the aromatic compounds listed in Figure 1A. Conjugation was monitored by emission of fluorescence (NBD), and by matrix-assisted laser desorption/ionization (MALDI) mass spectrometry (Figure S3).

Fluorescence emission spectra—Fluorescence-emission spectra were obtained by fixing the excitation wavelength at 470 nm. An emission spectrum of a sample lacking the fluorophore was subtracted from the spectrum of the equivalent sample containing the fluorophore. Fluorescence spectra of NBD were obtained upon incubation of NBD-labeled Fab (0.5 μM) with liposomes (total lipid concentration 250 μM) that contained 1.7 μM of the epitope peptide KKKNWFDITNWLWYIKLFIMIVGGLVKK.

Mass spectrometry—Prior to the measurement, all Fab preparations were desalted using ZipTip® C4 micro-columns (Millipore) (2 μL sample) with 0.5 μL SA buffer (sinapinic acid, 10 mg/ml in [70:30] Acetonitrile:Trifluoroacetic acid 0.1%), and arrayed onto a Ground Steel massive 384 target plate (Bruker Daltonics). Mass determinations were performed in a matrix-assisted laser desorption/ionization (MALDI), tandem time-of-flight (TOF/TOF) spectrometer Autoflex III (Bruker Daltonics). Mass calibration was performed externally with a Protein Calibration Standard 1 mixture (Bruker Daltonics) in the same mass range as the samples. Data acquisition, peak peaking and subsequent spectra analysis were performed using flexAnalysis 3.0 software (Bruker Daltonics).

Functional screening—Functional screening for the most effective chemical conjugates was carried out in pseudovirus (PsV)-based cell-entry assays (Bobardt et al., 2008). HIV-1 PsVs were produced by transfection of human kidney HEK293T cells with the full-length Env clone JRCSF (kindly provided by Jamie K. Scott and Naveed Gulzar, Simon Fraser University, BC, Canada) and the PVO.4 molecular clone (obtained from the AIDS Research and Reference Reagent Program (ARRRP)). Cells were co-transfected with vectors pWXLP-GFP and pCMV8.91, encoding a green fluorescent protein and an Env-deficient HIV-1 genome, respectively (provided by Patricia Villace, CSIC, Madrid, Spain). After 24 h, the medium was replaced with Optimem-Glutamax II (Invitrogen Ltd, Paisley, UK) without serum. Two days after transfection, the PsV particles were harvested, passed through 0.45 μm pore sterile filters (Millex® HV, Millipore NV, Brussels, Belgium) and finally concentrated by ultracentrifugation in a sucrose gradient. HIV entry was determined using $CD4^+CXCR4^+CCR5^+$ TZM-bl target cells (ARRRP, contributed by J. Kappes). To that end, HIV PsVs were first diluted to 10%–20% tissue culture infectious doses in DMEM supplemented with inactive serum, and added to the modified and WT Fabs. Infection levels after 72 hours were inferred from the number of GFP-positive cells as determined by flow cytometry using a BD FACSCalibur Flow Cytometer (Becton Dickinson Immunocytometry Systems, Mountain View, CA).

Binding to integral membrane Env by super-resolution fluorescence stimulated emission depletion (STED) microscopy—Purified virus particles were adhered to poly-L-lysine (Sigma) coated glass coverslips for 15 min. Coverslips were blocked using 2% fatty acid free bovine serum albumin (BSA) (Sigma)/PBS for 15 min. Fabs (25 ng/μL) were incubated for 1 h in blocking buffer and revealed upon incubation with anti-human Abberior STAR RED (KK114) conjugated Ab. Immuno-stained particles were washed and mounted in PBS, followed by STED analysis. All steps were carried out at RT.

Imaging was performed on a STED microscope based on a modified Abberior Instrument RESOLFT QUAD-P super-resolution microscope (Abberior Instruments GmbH). The fluorescence excitation and collection were performed using a 100 × /1.40 NA UPlanSApo oil immersion objective (Olympus Industrial, Southend-on-Sea, UK). The fluorescence signal was descanned, passed through an adjustable pinhole (Thorlabs Limited, Ely, UK) and detected by a single photon counting avalanche photo diode (SPCM-AQRH-13, Excelitas Techologies) with appropriate fluorescence filters (AHF Analysentechnik). All acquisition operations were controlled by Imspector software (Abberior Instruments). Resolution was typically around 40 nm. Emitted photons were recorded line by line in STED microscopy mode, and Vpr.eGFP was next imaged in confocal mode to determine the location of HIV-1 virions.

Image analysis was performed using Python scripting language and custom written functions, based on a previously developed program (Carravilla et al., 2019; Galiani et al., 2016). Individual viral particles were identified from the Vpr.eGFP channel using an intensity maximum finding algorithm on a Gaussian smoothed image ($\sigma = 2.0$). Detection of maxima was kept consistent throughout using a noise tolerance parameter of 10. A circular region (diameter, 20 pixels; 400 nm) was then superimposed on each detected location, and all of the regions were saved for subsequent analysis. For every detected region, a random location was also generated to sample areas where Vpr.eGFP staining and thus HIV-1 virions were not likely to be present. This was achieved by randomly translating each of the detected regions to a different point within a 90-pixel radius of the original location but constrained so as not to pick an existing region, which might contain another fragment of Vpr.eGFP fluorescence. This method was effective at finding random regions that were close to virions but not overlapping and so ensured accurate comparisons between virion-containing and nonvirion regions. These randomly perturbed regions were saved and their intensity subtracted from the intensity in virion (eGFP positive) regions.

Viral infection of primary CD4+ T cells—CD4+ T cells were purified (> 90%) from freshly isolated PBMCs by positive selection with antibody-coated magnetic beads (Easy-Sep Human CD4 Positive Selection Kit Ref.17852) using a RoboSep instrument (Stemcell Technology). Cells were cultured in RPMI 1640 containing GlutaMAX, 10% FCS, penicillin (10 UI/ml) and streptomycin (10 μg/ml) in the presence of IL-2 (Miltenyi) at 200 IU/ml and stimulated for three days with 4 μg/ml of PHA-L (Roche, Ref. 11249738001). CD4+ T cells were washed and seeded in triplicate in 96-U-well plate (100μl/well at 10^6/ml). WT or chemically-modified Fabs were added at different concentrations (dilutions of 10 to 10, range from 10 to 0.1 mg/ml) to the cultures, which were then exposed to HIV-1 BAL strain (R5) (10 ng p24/ml). After spinoculation at 1200 × g, 1 hour, the cells were incubated

at 37°C, 5% CO_2 for 72 h in presence of IL2. HIV infection levels of CD4+ T cells were monitored by intracellular p24 staining as previously described (Sáez-Cirión et al., 2010). Cells were stained for viability (AquaFluo, Invitrogen #L32957) and surface expression of CD3 (clone UCHT1, eFluor 450, eBiosciences, #480003642) and CD4 (clone OKT4, Alexa Fluor 700, Invitrogen,#56-0048-82). Cells were then fixed and permeabilized (BD Cytofix/Cytoperm) and stained for intracellular p24 (p24-FITC (clone KC57, Coulter). Cells were analyzed with a LSR II instrument (BD Bioscience) and the data processed with Kaluza Analysis software (v2.1, Beckman Coulter).

Standard assays for neutralization breadth—To evaluate the effects of chemical modification on the Ab capacity to neutralize a broad spectrum of HIV variants, a panel of PsVs was employed based on a previous study (Simek et al., 2009). Here, HIV-1 PsVs, were generated by co-transfection of 293T cells with Env plasmid DNA and the HIV-1 backbone plasmid pSG3ΔEnv (Wei et al., 2003), as previously described (Leaman et al., 2010). Env proteins and their sources were as follows: JRFL was from the NIH ARRRP; 92RW020, 94UG103, 92BR020, 92TH021, IAVI C22 and BG505 were from D. Burton (Scripps) and 16055 was from R. Wyatt (Scripps), and SIVmac239 was from J. Binley (SDBRI). HIV-2 7312A *env* was subcloned from the 7312A molecular clone plasmid (Gao et al., 1994) into pSVIIIexE7pA using KpnI-*Xho*I restriction sites as previously described (Zwick et al., 2001). Most genes encoding Env were contained in the plasmid pSVIII; ADA-CM, by exception was contained in pcDNA. Neutralization was determined using a single-cycle infectivity assay with $CD4^+CXCR4^+CCR5^+$ TZM-bl cells as target cells. Antibodies were added to virus in cell culture media (DMEM supplemented with 10% FBS, 2mM L-glutamine, 100 U/mL penicillin, and 100 mg/mL streptomycin) and incubated for 1h at 37°C prior to addition to target cells. Following a 72 h incubation at 37°C, cells were lysed, Bright-Glo luciferase reagent (Promega) was added, and luminescence in relative light units (RLUs) was measured using a Synergy H1 plate reader (BioTek).

QUANTIFICATION AND STATISTICAL ANALYSIS

STED images were analyzed and quantified using Python script language and custom written functions as detailed in the methods section. Statistical analysis was performed using OriginPro 2019. Two sample t tests were performed for values obtained in five independent experiments using two independent virus preparations.

Supplementary Material

Refer to Web version on PubMed Central for supplementary material.

ACKNOWLEDGMENTS

We are grateful to Professor Ueda (Kyushu University) for valuable advice. C.D. acknowledges RES (Red Española de Supercomputación) for providing computational resources. S.I. received a pre-doctoral fellowship from the Basque Government. P.C. acknowledges a research associate contract from the University of the Basque Country (DOCREC18/01) and a postdoctoral fellowship from the Basque Government (POS_2018_1_0066).This study was supported by the following grants: European Commission (790012 SI H2020-MSCA-IF-2017 to E.R., J.-P.J., and J.L.N.); US NIAID (NIH) (R01 AI143563 to M.B.Z.); James B. Pendleton Charitable Trust (to M.B.Z.); Grant-in-Aid for Scientific Research on Innovative Areas “Chemistry for Multimolecular Crowding Biosystems, JSPS KAKENHI (JP17H06349 to A.O.); JSPS KAKENHI (15K06962 and 20H03228 to J.M.M.C.); Spanish MINECO (BIO2015-64421-R and MINECO/AEI/FEDER, UE to J.L.N.); Spanish MCIU (RTI2018-095624-B-C21 and

MCIU/AEI/FEDER, UE to J.L.N.); and the Basque Government (IT1196-19) (to J.L.N.). C.E. acknowledges funding from Medical Research Council (MC_UU_12010/unit programs G0902418 and MC_UU_12025), Wolfson Foundation, Deutsche Forschungsgemeinschaft (Research unit 1905, Excellence Cluster Balance of the Microverse, Collaborative Research Centre 1278 Polytarget), Wellcome Institutional Strategic Support Fund, Oxford internal funds (EPA Cephalosporin Fund and John Fell Fund), and support from the Micron Oxford Advanced Bioimaging Unit (Wellcome Trust funding 107457/Z/15/Z). This research was undertaken, in part, thanks to funding from the CIFAR Azrieli Global Scholar program (to J.-P.J.) and the Canada Research Chairs program (950-231604 to J.-P.J.). This work was also supported by the Platform Project for Supporting Drug Discovery and Life Science Research (Basis for Supporting Innovative Drug Discovery and Life Science Research [BINDS] from AMED JP19am0101091).

REFERENCES

Bobardt MD, Cheng G, de Witte L, Selvaraj S, Chatterji U, Sanders Beer BE, Geijtenbeek TBH, Chisari FV, and Gallay PA (2008). Hepatitis C virus NS5A anchor peptide disrupts human immunodeficiency virus. Proc. Natl. Acad. Sci. USA 105, 5525–5530. [PubMed: 18378908]

Carravilla P, Chojnacki J, Rujas E, Insausti S, Largo E, Waithe D, Apellaniz B, Sicard T, Julien JP, Eggeling C, and Nieva JL (2019). Molecular recognition of the native HIV-1 MPER revealed by STED microscopy of single virions. Nat. Commun 10, 78. [PubMed: 30622256]

Crooks ET, Jiang P, Franti M, Wong S, Zwick MB, Hoxie JA, Robinson JE, Moore PL, and Binley JM (2008). Relationship of HIV-1 and SIV envelope glycoprotein trimer occupation and neutralization. Virology 377, 364–378. [PubMed: 18539308]

Darden T, York D, and Pedersen L (1993). Particle Mesh Ewald - an N.Log(N) Method for Ewald Sums in Large Systems. J. Chem. Phys 98, 10089–10092.

Feller SE, Zhang YH, Pastor RW, and Brooks BR (1995). Constant Pressure Molecular-Dynamics Simulation - the Langevin Piston Method. J. Chem. Phys 103, 4613–4621.

Flyak AI, Kuzmina N, Murin CD, Bryan C, Davidson E, Gilchuk P, Gulka CP, Ilinykh PA, Shen X, Huang K, et al. (2018). Broadly neutralizing antibodies from human survivors target a conserved site in the Ebola virus glycoprotein HR2-MPER region. Nat. Microbiol 3, 670–677. [PubMed: 29736037]

Galiani S, Waithe D, Reglinski K, Cruz-Zaragoza LD, Garcia E, Clausen MP, Schliebs W, Erdmann R, and Eggeling C (2016). Super-resolution Microscopy Reveals Compartmentalization of Peroxisomal Membrane Proteins. J. Biol. Chem 291, 16948–16962. [PubMed: 27311714]

Gao F, Yue L, Robertson DL, Hill SC, Hui H, Biggar RJ, Neequaye AE, Whelan TM, Ho DD, Shaw GM, et al. (1994). Genetic diversity of human immunodeficiency virus type 2: evidence for distinct sequence subtypes with differences in virus biology. J. Virol 68, 7433–7447. [PubMed: 7933127]

Hendriks D, Choi G, de Bruyn M, Wiersma VR, and Bremer E (2017). Antibody-Based Cancer Therapy: Successful Agents and Novel Approaches. Int. Rev. Cell Mol. Biol 331, 289–383. [PubMed: 28325214]

Heuck AP, Hotze EM, Tweten RK, and Johnson AE (2000). Mechanism of membrane insertion of a multimeric beta-barrel protein: perfringolysin O creates a pore using ordered and coupled conformational changes. Mol. Cell 6, 1233–1242. [PubMed: 11106760]

Hoff B, Strandberg E, Ulrich AS, Tieleman DP, and Posten C (2005). 2H-NMR study and molecular dynamics simulation of the location, alignment, and mobility of pyrene in POPC bilayers. Biophys. J 88, 1818–1827. [PubMed: 15596514]

Huang J, Ofek G, Laub L, Louder MK, Doria-Rose NA, Longo NS, Imamichi H, Bailer RT, Chakrabarti B, Sharma SK, et al. (2012). Broad and potent neutralization of HIV-1 by a gp41-specific human antibody. Nature 491, 406–412. [PubMed: 23151583]

Huarte N, Carravilla P, Cruz A, Lorizate M, Nieto-Garai JA, Kräusslich HG, Pérez-Gil J, Requejo-Isidro J, and Nieva JL (2016). Functional organization of the HIV lipid envelope. Sci. Rep 6, 34190. [PubMed: 27678107]

Hutchings CJ, Koglin M, Olson WC, and Marshall FH (2017). Opportunities for therapeutic antibodies directed at G-protein-coupled receptors. Nat. Rev. Drug Discov 16, 787–810. [PubMed: 28706220]

Hutchings CJ, Colussi P, and Clark TG (2019). Ion channels as therapeutic antibody targets. MAbs 11, 265–296. [PubMed: 30526315]

Irimia A, Sarkar A, Stanfield RL, and Wilson IA (2016). Crystallographic Identification of Lipid as an Integral Component of the Epitope of HIV Broadly Neutralizing Antibody 4E10. Immunity 44, 21–31. [PubMed: 26777395]

Irimia A, Serra AM, Sarkar A, Jacak R, Kalyuzhniy O, Sok D, Saye-Francisco KL, Schiffner T, Tingle R, Kubitz M, et al. (2017). Lipid interactions and angle of approach to the HIV-1 viral membrane of broadly neutralizing antibody 10E8: Insights for vaccine and therapeutic design. PLoS Pathog 13, e1006212. [PubMed: 28225819]

Isenegger PG, and Davis BG (2019). Concepts of Catalysis in Site-Selective Protein Modifications. J. Am. Chem. Soc 141, 8005–8013. [PubMed: 30974939]

Jo S, Kim T, Iyer VG, and Im W (2008). CHARMM-GUI: a web-based graphical user interface for CHARMM. J. Comput. Chem 29, 1859–1865. [PubMed: 18351591]

Jorgensen WL, Chandrasekhar J, Madura JD, Impey RW, and Klein ML (1983). Comparison of Simple Potential Functions for Simulating Liquid Water. J. Chem. Phys 79, 926–935.

Kawai T, Caaveiro JMM, Abe R, Katagiri T, and Tsumoto K (2011). Catalytic activity of MsbA reconstituted in nanodisc particles is modulated by remote interactions with the bilayer. FEBS Lett 585, 3533–3537. [PubMed: 22020218]

Klauda JB, Venable RM, Freites JA, O'Connor JW, Tobias DJ, Mondragon-Ramirez C, Vorobyov I, MacKerell AD Jr., and Pastor RW (2010). Update of the CHARMM all-atom additive force field for lipids: validation on six lipid types. J. Phys. Chem. B 114, 7830–7843. [PubMed: 20496934]

Klein C, Lammens A, Schäfer W, Georges G, Schwaiger M, Mössner E, Hopfner KP, Umaña P, and Niederfellner G (2013). Epitope interactions of monoclonal antibodies targeting CD20 and their relationship to functional properties. MAbs 5, 22–33. [PubMed: 23211638]

Krall N, da Cruz FP, Boutureira O, and Bernardes GJ (2016). Site-selective protein-modification chemistry for basic biology and drug development. Nat. Chem 8, 103–113. [PubMed: 26791892]

Krebs SJ, Kwon YD, Schramm CA, Law WH, Donofrio G, Zhou KH, Gift S, Dussupt V, Georgiev IS, Schatzle S, et al. (2019). Longitudinal Analysis Reveals Early Development of Three MPER-Directed Neutralizing Antibody Lineages from an HIV-1-Infected Individual. Immunity 50, 677–691. [PubMed: 30876875]

Kwon YD, Chuang GY, Zhang B, Bailer RT, Doria-Rose NA, Gindin TS, Lin B, Louder MK, McKee K, O'Dell S, et al. (2018). Surface-Matrix Screening Identifies Semi-specific Interactions that Improve Potency of a Near Pan-reactive HIV-1-Neutralizing Antibody. Cell Rep 22, 1798–1809. [PubMed: 29444432]

Leaman DP, Kinkead H, and Zwick MB (2010). In-solution virus capture assay helps deconstruct heterogeneous antibody recognition of human immunodeficiency virus type 1. J. Virol 84, 3382–3395. [PubMed: 20089658]

Leaman DP, and Zwick MB (2013). Increased functional stability and homogeneity of viral envelope spikes through directed evolution. PLoS Pathog 9, e1003184. [PubMed: 23468626]

Lee JH, Park CK, Chen G, Han Q, Xie RG, Liu T, Ji RR, and Lee SY (2020). Retraction. Cell 181, 1695. [PubMed: 32589960]

Lee JH, Ozorowski G, and Ward AB (2016). Cryo-EM structure of a native, fully glycosylated, cleaved HIV-1 envelope trimer. Science 351, 1043–1048. [PubMed: 26941313]

Loura LM, do Canto AM, and Martins J (2013). Sensing hydration and behavior of pyrene in POPC and POPC/cholesterol bilayers: a molecular dynamics study. Biochim. Biophys. Acta 1828, 1094–1101. [PubMed: 23274277]

MacKerell AD, Bashford D, Bellott M, Dunbrack RL, Evanseck JD, Field MJ, Fischer S, Gao J, Guo H, Ha S, et al. (1998). All-atom empirical potential for molecular modeling and dynamics studies of proteins. J. Phys. Chem. B 102, 3586–3616. [PubMed: 24889800]

McDonald SK, and Fleming KG (2016). Aromatic Side Chain Water-to-Lipid Transfer Free Energies Show a Depth Dependence across the Membrane Normal. J. Am. Chem. Soc 138, 7946–7950. [PubMed: 27254476]

Munro JB, Gorman J, Ma X, Zhou Z, Arthos J, Burton DR, Koff WC, Courter JR, Smith AB 3rd, Kwong PD, et al. (2014). Conformational dynamics of single HIV-1 envelope trimers on the surface of native virions. Science 346, 759–763. [PubMed: 25298114]

Pahuja KB, Nguyen TT, Jaiswal BS, Prabhash K, Thaker TM, Senger K, Chaudhuri S, Kljavin NM, Antony A, Phalke S, et al. (2018). Actionable Activating Oncogenic ERBB2/HER2 Transmembrane and Juxtamembrane Domain Mutations. Cancer Cell 34, 792–806. [PubMed: 30449325]

Phillips JC, Braun R, Wang W, Gumbart J, Tajkhorshid E, Villa E, Chipot C, Skeel RD, Kalé L, and Schulten K (2005). Scalable molecular dynamics with NAMD. J. Comput. Chem 26, 1781–1802. [PubMed: 16222654]

Pinto D, Fenwick C, Caillat C, Silacci C, Guseva S, Dehez F, Chipot C, Barbieri S, Minola A, Jarrossay D, et al. (2019). Structural Basis for Broad HIV-1 Neutralization by the MPER-Specific Human Broadly Neutralizing Antibody LN01. Cell Host Microbe 26, 623–637. [PubMed: 31653484]

Rantalainen K, Berndsen ZT, Antanasijevic A, Schiffner T, Zhang X, Lee WH, Torres JL, Zhang L, Irimia A, Copps J, et al. (2020). HIV-1 Envelope and MPER Antibody Structures in Lipid Assemblies. Cell Rep 31, 107583. [PubMed: 32348769]

Rujas E, Gulzar N, Morante K, Tsumoto K, Scott JK, Nieva JL, and Caaveiro JM (2015). Structural and Thermodynamic Basis of Epitope Binding by Neutralizing and Nonneutralizing Forms of the Anti-HIV-1 Antibody 4E10. J. Virol 89, 11975–11989. [PubMed: 26378169]

Rujas E, Caaveiro JM, Partida-Hanon A, Gulzar N, Morante K, Apellániz B, García-Porras M, Bruix M, Tsumoto K, Scott JK, et al. (2016). Structural basis for broad neutralization of HIV-1 through the molecular recognition of 10E8 helical epitope at the membrane interface. Sci. Rep 6, 38177. [PubMed: 27905530]

Rujas E, Caaveiro JM, Insausti S, García-Porras M, Tsumoto K, and Nieva JL (2017). Peripheral Membrane Interactions Boost the Engagement by an Anti-HIV-1 Broadly Neutralizing Antibody. J. Biol. Chem 292, 5571–5583. [PubMed: 28213514]

Rujas E, Leaman DP, Insausti S, Ortigosa-Pascual L, Zhang L, Zwick MB, and Nieva JL (2018). Functional Optimization of Broadly Neutralizing HIV-1 Antibody 10E8 by Promotion of Membrane Interactions. J. Virol 92, e02249–17. [PubMed: 29386285]

Sáez-Cirión A, Shin SY, Versmisse P, Barré-Sinoussi F, and Pancino G (2010). Ex vivo T cell-based HIV suppression assay to evaluate HIV-specific CD8+ T-cell responses. Nat. Protoc 5, 1033–1041. [PubMed: 20539279]

Sakamoto S, and Hamachi I (2019). Recent Progress in Chemical Modification of Proteins. Anal. Sci 35, 5–27. [PubMed: 30318491]

Shepard LA, Heuck AP, Hamman BD, Rossjohn J, Parker MW, Ryan KR, Johnson AE, and Tweten RK (1998). Identification of a membrane-spanning domain of the thiol-activated pore-forming toxin Clostridium perfringens perfringolysin O: an a-helical to beta-sheet transition identified by fluorescence spectroscopy. Biochemistry 37, 14563–14574. [PubMed: 9772185]

Simek MD, Rida W, Priddy FH, Pung P, Carrow E, Laufer DS, Lehrman JK, Boaz M, Tarragona-Fiol T, Miiro G, et al. (2009). Human immunodeficiency virus type 1 elite neutralizers: individuals with broad and potent neutralizing activity identified by using a high-throughput neutralization assay together with an analytical selection algorithm. J. Virol 83, 7337–7348. [PubMed: 19439467]

Stiegler G, Kunert R, Purtscher M, Wolbank S, Voglauer R, Steindl F, and Katinger H (2001). A potent cross-clade neutralizing human monoclonal antibody against a novel epitope on gp41 of human immunodeficiency virus type 1. AIDS Res. Hum. Retroviruses 17, 1757–1765. [PubMed: 11788027]

Tuckerman M, Berne BJ, and Martyna GJ (1992). Reversible Multiple Time Scale Molecular-Dynamics. J. Chem. Phys 97, 1990–2001.

Valle-Casuso JC, Angin M, Volant S, Passaes C, Monceaux V, Mikhailova A, Bourdic K, Avettand-Fenoel V, Boufassa F, Sitbon M, et al. (2019). Cellular Metabolism Is a Major Determinant of HIV-1 Reservoir Seeding in CD4(+) T Cells and Offers an Opportunity to Tackle Infection. Cell Metab 29, 611–626. [PubMed: 30581119]

Verlet L (1967). Computer Experiments on Classical Fluids. I. Thermodynamical Properties of Lennard-Jones Molecules. Phys. Rev 159, 98.

Walker LM, and Burton DR (2018). Passive immunotherapy of viral infections: ‘super-antibodies’ enter the fray. Nat. Rev. Immunol 18, 297–308. [PubMed: 29379211]

Wei X, Decker JM, Liu H, Zhang Z, Arani RB, Kilby JM, Saag MS, Wu X, Shaw GM, and Kappes JC (2002). Emergence of resistant human immunodeficiency virus type 1 in patients receiving fusion inhibitor (T-20) monotherapy. Antimicrob. Agents Chemother 46, 1896–1905. [PubMed: 12019106]

Wei X, Decker JM, Wang S, Hui H, Kappes JC, Wu X, Salazar-Gonzalez JF, Salazar MG, Kilby JM, Saag MS, et al. (2003). Antibody neutralization and escape by HIV-1. Nature 422, 307–312. [PubMed: 12646921]

White SH, and Wimley WC (1999). Membrane protein folding and stability: physical principles. Annu. Rev. Biophys. Biomol. Struct 28, 319–365. [PubMed: 10410805]

White SH, Ladokhin AS, Jayasinghe S, and Hristova K (2001). How membranes shape protein structure. J. Biol. Chem 276, 32395–32398. [PubMed: 11432876]

Williams LD, Ofek G, Schätzle S, McDaniel JR, Lu X, Nicely NI, Wu L, Lougheed CS, Bradley T, Louder MK, et al. (2017). Potent and broad HIV-neutralizing antibodies in memory B cells and plasma. Sci. Immunol 2, eaal2200. [PubMed: 28783671]

Wimley WC, and White SH (1996). Experimentally determined hydrophobicity scale for proteins at membrane interfaces. Nat. Struct. Biol 3, 842–848. [PubMed: 8836100]

Xu SZ, Zeng F, Lei M, Li J, Gao B, Xiong C, Sivaprasadarao A, and Beech DJ (2005). Generation of functional ion-channel tools by E3 targeting. Nat. Biotechnol 23, 1289–1293. [PubMed: 16170312]

Yau WM, Wimley WC, Gawrisch K, and White SH (1998). The preference of tryptophan for membrane interfaces. Biochemistry 37, 14713–14718. [PubMed: 9778346]

Zhang L, Irimia A, He L, Landais E, Rantalainen K, Leaman DP, Vollbrecht T, Stano A, Sands DI, Kim AS, et al.; IAVI Protocol G Investigators (2019). An MPER antibody neutralizes HIV-1 using germline features shared among donors. Nat. Commun 10, 5389. [PubMed: 31772165]

Zwick MB, Wang M, Poignard P, Stiegler G, Katinger H, Burton DR, and Parren PW (2001). Neutralization synergy of human immunodeficiency virus type 1 primary isolates by cocktails of broadly neutralizing antibodies. J. Virol 75, 12198–12208. [PubMed: 11711611]

Zwick MB, Kelleher R, Jensen R, Labrijn AF, Wang M, Quinnan GV Jr., Parren PW, and Burton DR (2003). A novel human antibody against human immunodeficiency virus type 1 gp120 is V1, V2, and V3 loop dependent and helps delimit the epitope of the broadly neutralizing antibody immunoglobulin G1 b12. J Virol 77, 6965–6978. [PubMed: 12768015]

Highlights

- Aromatic compounds are shown to interact with the HIV-lipid membrane interface
- HIV antibody 10E8, which binds a membrane-embedded epitope, is chemically modified
- 10E8 potency improves >100-fold by site-selective labeling with aromatic compounds
- The same aromatic grafting procedure is successfully applied to a second antibody

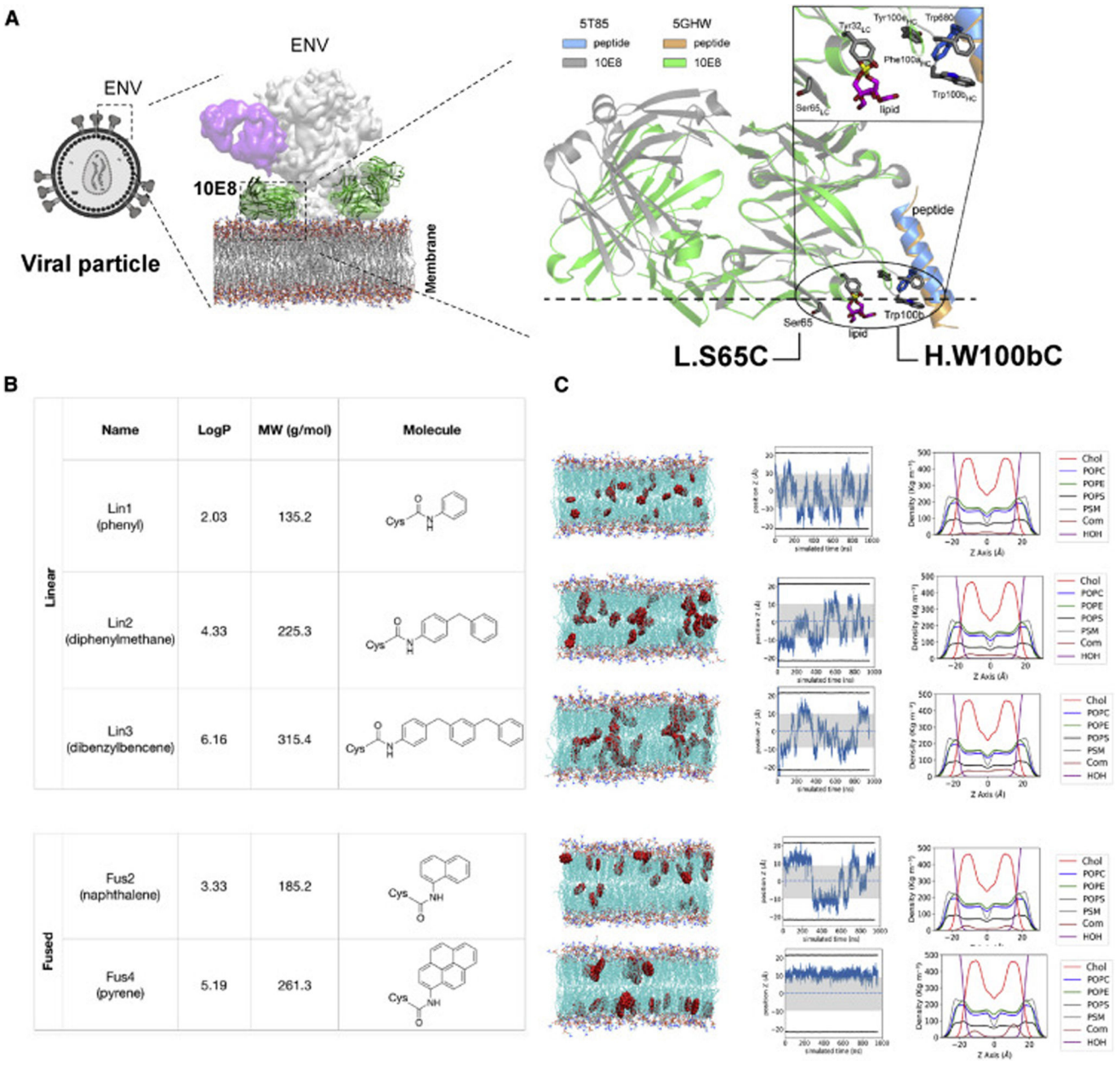

Figure 1. Chemical Modification of Fab 10E8 at Selected Residues within the Membrane-Proximal Area

(A) Structure-guided selection of residues within the Fab surface that accommodates the viral membrane upon engagement with the epitope. The positions of the L.S65 and H.W100b residues selected for substitution with Cys are indicated (see also Figure S1).

(B) Basic properties and structural formulae of the synthetic aromatic compounds Lin1, Lin2, Lin3, Fus2, and Fus4 selected for the chemical modification of the antibody.

(C) Molecular dynamics simulations of the aromatic moieties composing Lin1, Lin2, Lin3, Fus2, and Fus4 in virus-like lipid bilayers: Left: snapshots taken at 500 ns. Center: positions of the center of mass of the molecules along the z axis over time (representative examples of

single molecules are shown); the position of the phosphate groups is followed by the black thick line. Right: mass density profiles of lipids and compounds in the VL lipid bilayer. See also Figures S2 and S3 and Table S1.

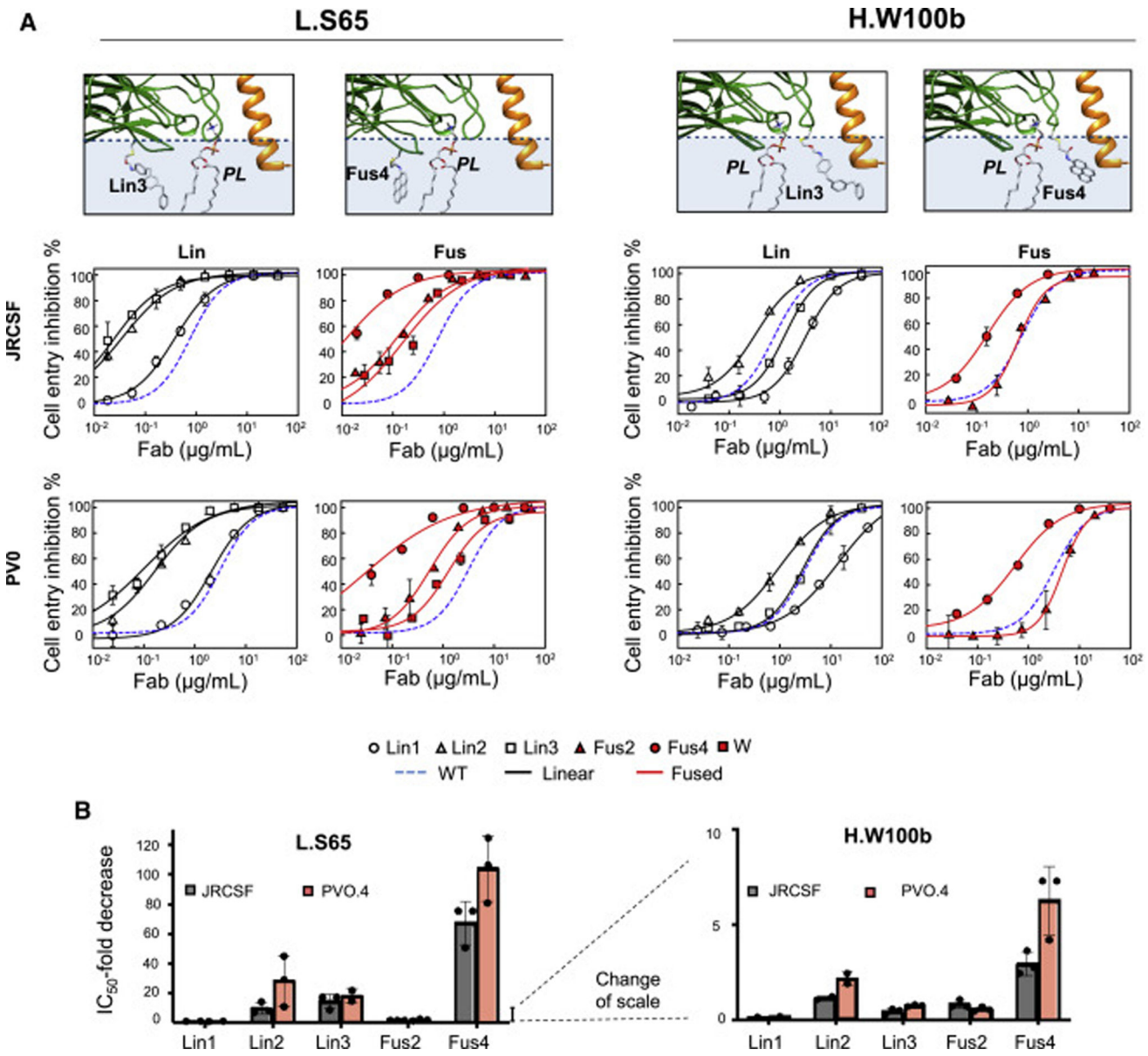

Figure 2. Effect of Site-Specific Chemical Modification with Aromatics on the Anti-Viral Activity of Fab 10E8

(A) Cell-entry inhibition assays against JRCSF (Tier-2) and PVO.4 (Tier-3) PsVs comparing unmodified WT Fab with Fabs modified with the synthetic aromatic compounds. The top panels depict the position of the modifications with Lin3 or Fus4 (see also Figure S4). PL denotes the position of a phospholipid molecule added to mark the level of the membrane interface. In the dose-response curves below, the dotted blue lines follow the activity of the WT Ab. Modifications of the linear and fused series are shown in black and red solid lines, respectively. Empty circles, triangles, and squares correspond to Lin1, Lin2, and Lin3, respectively. Data for Fus2, Fus4, and Trp are shown with red-filled circles, triangles, and squares, respectively, and correspond to mean values (±SD) from two replicate wells in a representative experiment.

(B) Increases in potency over the WT Ab (mean IC_{50} fold decrease ± SD), as determined from cell-entry inhibition data, are shown as a function of the position and the compound used for chemical modification. IC_{50} values were interpolated from dose-response curves obtained from three independent experiments as those shown in (A).

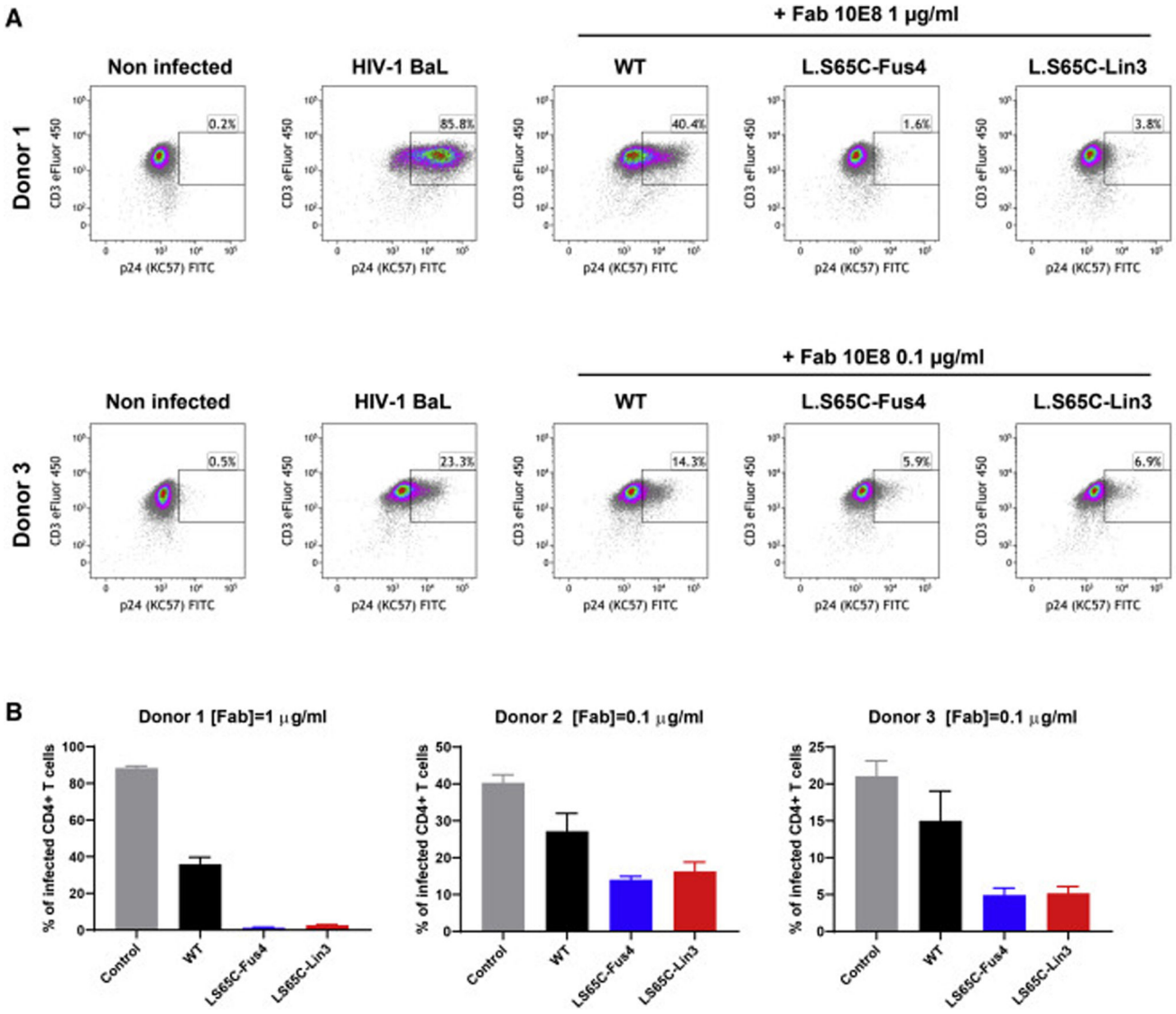

Figure 3. Block of Primary CD4$^+$ T Cell Infection by Chemically Modified Fab 10E8

(A) Levels of intracellular HIV-1 p24, determined by flow cytometry, in CD4$^+$ T cells isolated from donor 1 and donor 2 three days after infection with HIV-1 BaL. Infections were done in the absence or in presence of WT, L.S65C-Fus4, or L.S65C-Lin3 versions of 10E8 Fab.

(B) Means and SD values of experiments (n = 3 replicates) conducted with cells from 3 donors.

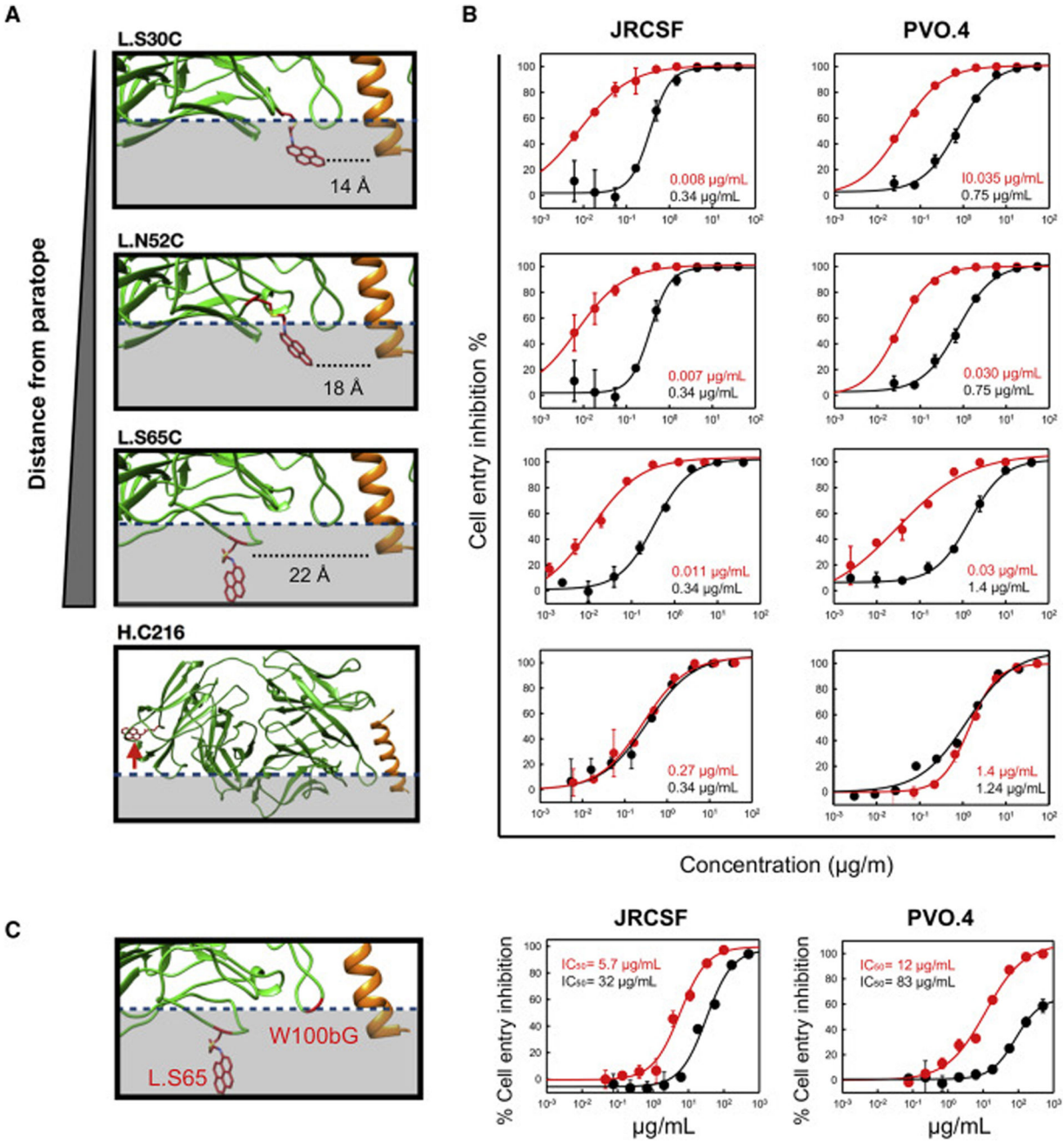

Figure 4. Effects of Fus4 Conjugated at Different Membrane-Proximal Sites

(A) Lateral views displaying the positions of the residues chemically modified with Fus4 (residues depicted in red) and the bound epitope-peptide (helix depicted in orange). Distances to the Ca-s of modified Fab residues were calculated from that of Lys683 at the bound helical epitope. The bottom panel displays the position of H.216C used as negative control for Fab-membrane interaction.

(B) Comparison of the antiviral activities of 10E8 Fabs modified with Fus4 at the different membrane-proximal positions indicated in the previous panels. The left and right panels correspond to the entry inhibition assay using JRCSF and PVO.4 strains, respectively. Solid

black and red lines (and symbols) correspond to unmodified and chemically modified antibody, respectively. Otherwise, same conditions as in Figure 2A.
(C) Effects of L.S65C-Fus4 modification on the Ab carrying the deleterious H.W100G mutation (see also Figure S5). Symbols and lines are defined as in (B).

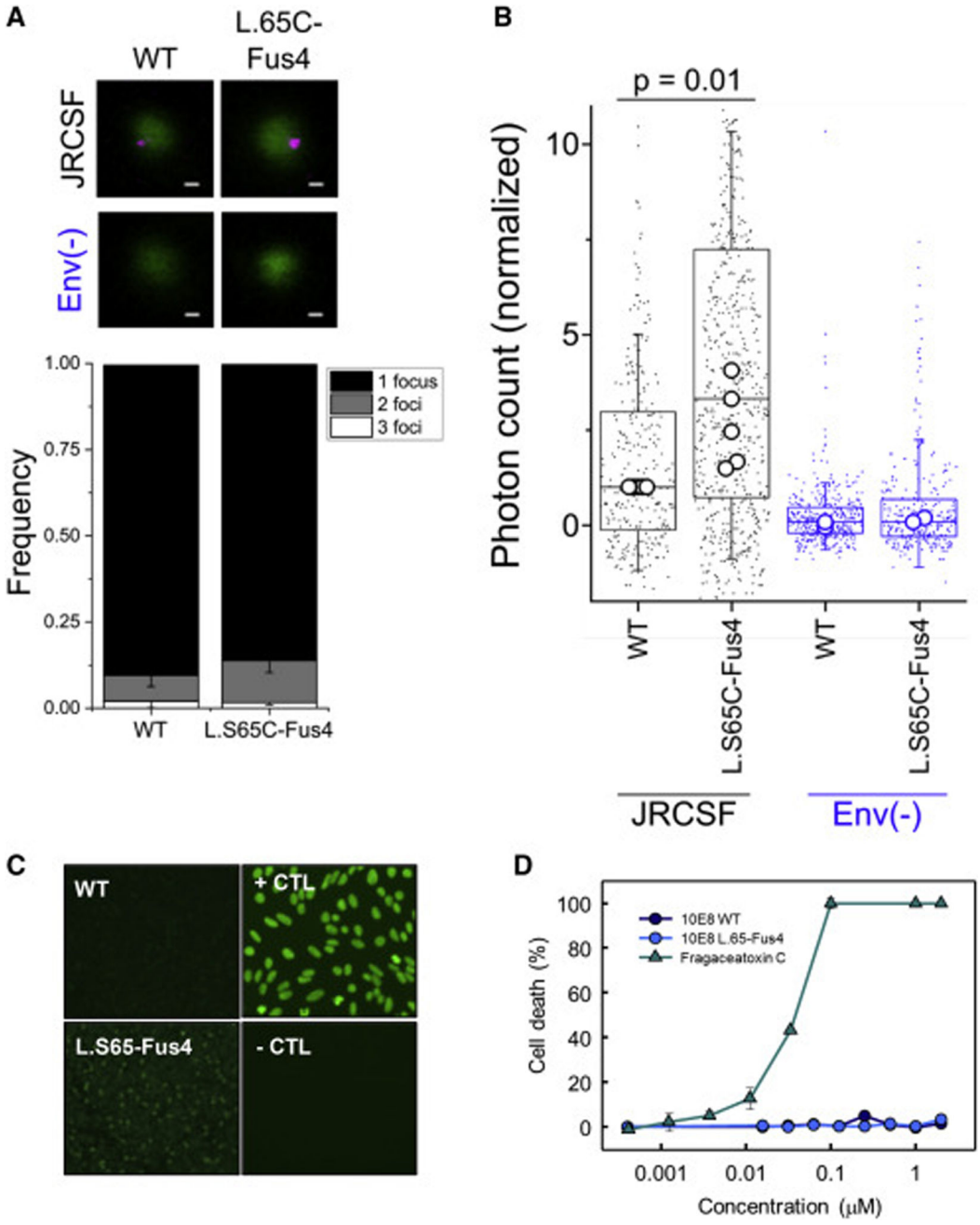

Figure 5. Binding Specificity of Chemically Modified Fab

(A) Binding to the integral membrane Env antigen by STED microscopy. Top: representative images of the binding of antibodies (KK114, STED modus, magenta) in the presence of Env JR-CSF or Env(–) HIV-1 virions (Vpr.GFP, confocal modus, green). Scale bars, 100 nm. Bottom: distribution of the number of antibody foci detected per individual Env JR-CSF virions.

(B) Emission intensity of WT and 10E8 L.S65C-Fus4 antibodies measured on individual Env JR-CSF (black) and Env(–) (blue) HIV-1 virions as determined from the STED microscopy images (from left to right, n = 282, 629, 369, and 315). The intensity was

normalized to that of 10E8 WT after background signal subtraction. Points represent normalized photon counts obtained for single virions. Circles represent median photon counts of each independent experiment, which were used for hypothesis testing. Two sample t tests were performed for values obtained in five independent experiments using two independent virus preparations. Results are additionally shown in boxplots (center line, median; box, interquartile range [IQR]; whiskers, SD).

(C) Fus4 effect on polyreactivity (see also Figure S7). Panels correspond to an immunofluorescence staining experiment using Fab 10E8 WT and chemically modified 10E8 L.S65C-Fus4 against HEp-2 cells.

(D) Absence of toxicity induced by chemically modified Fab on TZM-bl host cells. The CytoTox 96, non-radioactive cytotoxicity assay (Promega) was carried out following the instructions of the manufacturer. The cytolytic toxin fragaceatoxin C was used as positive control. Mean values (±SD) from three replicates are shown.

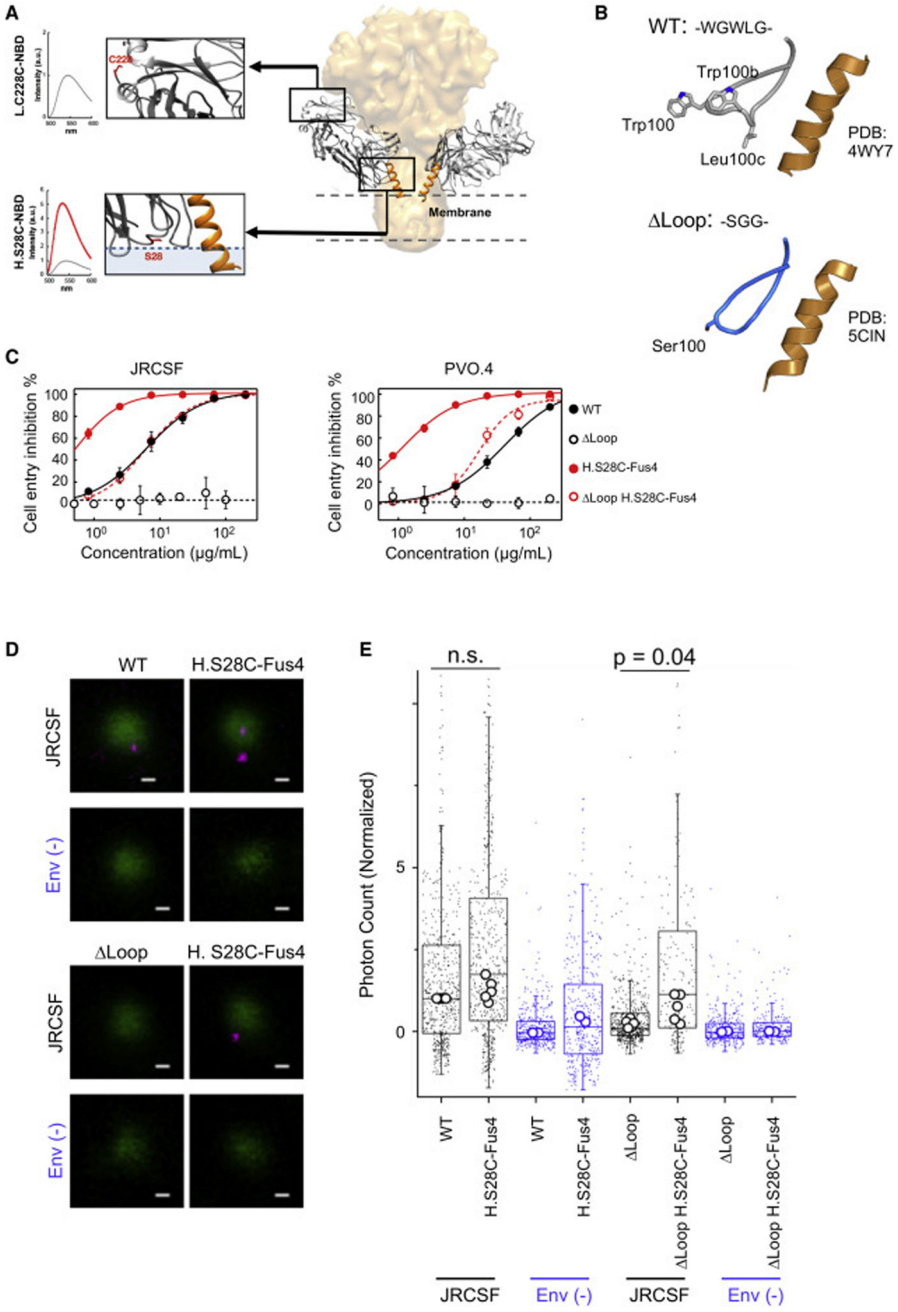

Figure 6. Effects of Fus4 Modification of the Membrane-Proximal Area in a Second Antibody

(A) Structural model of Fab 4E10 interacting with the Env complex. Fab was chemically modified at positions H.S28 or H.C228. These positions are predicted to interact with the membrane or remain solvent-exposed, respectively, upon engagement with MPER epitope. The interaction between Fab labeled with NBD and proteoliposomes was monitored by fluorescence.

(B) Schematics displaying the effects of ΔLoop mutation on the sequence and structure of the 4E10 HCDR3 loop.

(C) Anti-viral activities of the Fab 4E10 (filled symbols and continuous lines) and its nonfunctional variant ΔLoop (empty symbols and dotted lines). The anti-viral activity of H.S28C mutants modified with Fus4 on a WT background (active antibody) and on the inactive background (ΔLoop) are compared (see also Table S2). Red traces and symbols correspond to the chemically modified Fabs. Otherwise, same conditions as in Figure 2A.
(D) Representative images of Fabs 4E10 by STED microscopy (KK114, STED mode, magenta) in the presence of Env JR-CSF or Env(–) HIV-1 virions (Vpr.GFP, confocal modus, green). Scale bars, 100 nm.
(E) Antibody emission intensity as determined from STED microcopy images for Fabs 4E10, 4E10 H.S28C-Fus4, ΔLoop, and ΔLoop H.S28C-Fus4 interacting with Env JR-CSF or Env(–) HIV-1 virions (from left to right, n = 606, 581, 424, 397, 572, 198, 341, and 254). Otherwise, same conditions as in Figure 5B.

Table 1.

Fus4 Conjugation-Induced 10E8 Neutralization Improvement against a Variety of HIV Isolates

			10E8 IC_{50} (μg/mL)		
	Clade	**Tier**	**WT**	**L.S65C-Fus4**	**Fold Enhancement**
92UG103	A	2	0.37	0.015	25
92BR020	B	2	0.19	0.0046	41
IAVI C22	C	2	0.14	0.0002	708
92RW020	A	2	0.98	0.048	20
92TRH021	AE	2	0.016	0.00006	286
16055	C	2	0.22	0.0011	207
BG505	A	2	2.1	0.27	7.7
ADA-CM	B	2	0.15	0.0046	33
JRFL	B	2	0.015	0.000099	151
HIV-2	HIV-2	2	>5	>5	
SIVmac239	SIV	2	>5	>5	

IC_{50} values were interpolated from dose-response curves (see also Figure S6).

KEY RESOURCES TABLE

REAGENT or RESOURCE	SOURCE	IDENTIFIER
Antibodies		
Donkey anti-Human IgG Abberior STAR RED	Abberior	STRED-1054; RRID: Not defined
Goat anti-Human IgG, AP	Invitrogen	31312; RRID: AB_228274
Anti-Human IgG (Fab specific)	Sigma	I5260; RRID:AB_260206
Mouse anti-goat IgG-HRP	Santa Cruz Biotechnology	sc-2354; RRID:AB_628490
CD3-eFluor450	eBiosciences	Cat#48-0036-42 (SK7); RRID:AB_11217677
CD4-alexaFluor700	eBioscience	Cat#56-0048-82 (OKT-4); RRID:AB_657741
Anti-HIV-1 Core Antigen Antibody-FITC	Beckman Coulter	Cat#6604665 (KC57); RRID:AB_1575987
Bacterial and Virus Strains		
E. coli T7Shuffle	New England Biolabs	C3026J
HIV-1 Bal strain (R5)	NIH AIDS reagent program	Cat#510
Biological Samples		
Blood samples from non-infected donors	Etablissement Français du sang	https://dondesang.efs.sante.fr/
Chemicals, Peptides, and Recombinant Proteins		
2-Iodo-N-phenylacetamide (Lin1)	Ark Pharm	AK148507
2-Iodo-N-(pyren-1-yl) acetamide (Fus4)	Life Technologies	P29
gp41 MPER peptide	ProteoGenix	N/A
1-palmitoyl-2-oleoylphosphatidylcholine (POPC)	Avanti Polar Lipids	42773
1-palmitoyl-2-oleoylphosphatidylethanolamine (POPE)	Avanti Polar Lipids	01991
1-palmitoyl-2-oleoylphosphatidylserine (POPS)	Avanti Polar Lipids	840034C
N-palmitoylsphingomyelin (SM)	Avanti Polar Lipids	85615
Cholesterol (Chol)	Avanti Polar Lipids	C8667
DNase I	PanReac AppliChem	A3778,0010
EDTA-free protease inhibitor mixture	Roche	11873580001
IANBD Amide (N,N'-Dimethyl-N-(Iodoacetyl)-N'-(7-Nitrobenz-2-Oxa-1,3-Diazol-4-yl)Ethylenediamine)	Thermo Scientific	D2004
MEM Non-essential Amino Acid Solution	Thermo Scientific	11140050
Sodium Pyrubate	Thermo Scientific	11360070
Opti-MEM I Reduced-Serum Medium	Thermo Scientific	11058021
KOD-Plus mutagenesis kit	Toyobo	SMK-101
Bright-Glo luciferase reagent	Promega	E2610
PEI, MW 25 kDa	Polysciences	23966–1
DMEM Growth Medium	Life Technologies	10313–039
Fetal Bovine Serum	Life Technologies	10437–028
NuPAGE 3–8% Tris-acetate Gels	Life Technologies	EA03755BOX
Tris-glycine Native Sample Buffer	Life Technologies	LC2673
Coomassie Brilliant Blue G250	Sigma	27815
n-Dodecyl-beta-Maltoside (DDM)	Pierce	89903

REAGENT or RESOURCE	SOURCE	IDENTIFIER
ECL Plus Western Blotting Substrate	Pierce	32132
Sinapinic acid [4-Hydroxy-3,5-dimethoxycinnamic acid] MALDI matrix	Alfa Aesar	A15676
Trifluoroacetic acid	Thermo scientific	28904
Water, Optima LC/MS grade	Fischer chemical	W6-1
Acetonitrile, Optima LC/MS grade	Fischer chemical	A955-212
Protein Calibration Standard 1 mixture	Bruker Daltonics	206355
Poly-L-lysine solution	Sigma-Aldrich	P8920
Bovine Serum Albumin (fatty acid free)	Sigma-Aldrich	A7030
RPMI 1640 GlutaMAX	GIBCO	Cat#61870-010
PBS1x without calcium and magnesium	Thermo Fisher	Cat#12037539
Fetal Calf Serum	Eurobio	Cat#CVFSVF00-01
PenStrep	GIBCO	Cat#15140-122
Lymphocyte Separation Medium (LSM)	Eurobio	Cat#CMSMSL01-01
Human IL-2 IS premium grade	Miltenyi	Cat#130-097-748
Phytohemagglutinin-L PHA-L	Roche	Cat#11249738001
Fixation/PermeabilizationSolution Kit (Cytofix/Cytoperm)	BD Biosciences	Cat#554714
4% paraformaldehyde	Thermo Fisher	Cat#J61899
Critical Commercial Assays		
LIVE/DEADTM Violet Viability dye	Thermo Fisher	Cat#L34955
Kallestad HEp-2 Complete Kits	BioRad	32583
EasySep Human CD4 positive selection kit II	Stem Cell Technology	Cat#17852
HIV-1 p24 enzyme-linked immunosorbent assay	XpressBio	Cat#XB-1000
Experimental Models: Cell Lines		
Human: HEK293T Cells	ATCC	CRL-3216
Human: TZM-bl Cells	NIH AIDS Reagent Program	8129
Recombinant DNA		
pCOLADuet-1 expression plasmid	Sigma-Aldrich	71406
10E8 Fab pCOLADuet-1 wild-type and mutants	This paper	N/A
4E10 Fab pCOLADuet-1 wild-type and mutants	This paper	N/A
pWXLP-GFP	Patricia Villacé, CSIC	N/A
pCMV8.91	Patricia Villacé, CSIC	N/A
PVO, clone 4 (SVPB11) Expression plasmid	NIH AIDS Reagent Program	11022
JRCSF Expression plasmid	Jamie Scott, SFU	N/A
pSG3ΔEnv	NIH AIDS Reagent Program	11051
ADA.CM Expression plasmid	Leaman et al., 2013	N/A
92RW020.5 Expression plasmid	NIH AIDS Reagent Program	3097
94UG103 Expression plasmid	D. Burton, Scripps; Simek et al., 2009	N/A
92BR020 Expression plasmid	NIH AIDS Reagent Program	1780
92TH021 Expression plasmid	D. Burton, Scripps; Simek et al., 2009	N/A

REAGENT or RESOURCE	SOURCE	IDENTIFIER
IAVI C22 Expression plasmid	D. Burton, Scripps; Simek et al., 2009	N/A
BG505 Expression plasmid	NIH AIDS Reagent Program	11518
JRFL Expression plasmid	Zwick et al., 2003	N/A
SIVmac239 Expression plasmid	J. Binley, SDBRI; Crooks et al., 2008	N/A
HIV-2 7312A Expression plasmid	Zhang et al., 2019	N/A
pEGFP.Vpr	NIH AIDS Reagent Program	11386
Software and Algorithms		
Image Lab	Bio-Rad	N/A
Prism	GraphPad	N/A
flexControl 3.0	Bruker Daltonics	N/A
flexAnalysis 3.0	Bruker Daltonics	N/A
NAMD2.12	Phillips et al., 2005	N/A
Pymol Molecular Graphics System	Schrödinger	N/A
CHARMM GUI	Jo et al., 2008	http://www.charmm-gui.org/
STED analysis program	Galiani et al., 2016	https://doi.org/10.5281/zenodo.1465920.
OriginPro 2019b (9.6.5.169)	OriginLab Corporation	N/A
biorender	biorender.com	https://biorender.com/
Other		
ZipTip® C4 micro-columns	Millipore	ZTC04S096
Ground Steel massive 384 MALDI target plate	Bruker Daltonics	8074115
Nickel-nitrilotriacetic acid (Ni-NTA) affinity column	GE-Healthcare	10431065
MonoS ion exchange chromatography (IEC) column	GE-Healthcare	17516801